



university of
 groningen

Catalytic hydrogenation of levulinic acid to γ -valerolactone in a trickle bed reactor.

Analysis of mass transfer resistance and kinetics

MASTER THESIS
MEINE KOESLAG
S1629697

SUPERVISOR: DR. J. YUE
SECOND SUPERVISOR: PROF. DR. IR. H.J. HEERES
DAILY SUPERVISOR: IR. A. HOMMES

RIJKS UNIVERSITEIT GRONINGEN
DEPARTMENT OF CHEMICAL ENGINEERING

Abstract

In the search for alternatives for fossil fuels chemicals, biobased platform chemicals can play an integral role. One important bio-based platform chemical is γ -valerolactone (GVL) that can be used as a feed for solvents, bulk chemicals and intermediates for fine chemicals. GVL can be synthesized from another platform chemical: levulinic acid (LA). In this study, the rate limiting step of the hydrogenation of levulinic acid to GVL over 0.5 wt% Ru/C catalysts has been investigated in a continuous flow trickle bed reactor (volume: 4 mL; inner diameter: 10 mm). The reaction has been performed under a hydrogen pressure at 45 bar with an inlet LA concentration of 1.2 mol/L. A series of experiments were performed with varying reaction temperature (80 - 100 °C), flow rate of pure hydrogen (1.5 – 2.5 mol/min) and catalyst amount (0.4 – 1.8 g). Two catalyst particle sizes were used: coarse ($1.25 \text{ mm} < d_p < 2.5 \text{ mm}$) and fine ($0.5 \text{ mm} < d_p < 1.25 \text{ mm}$).

The results of experiments were compared with a simplified numerical model for the reaction rate. The numerical model was based on an equation derived to distinguish between gas absorption limitations, limitations from diffusion within the catalyst and kinetic limitations. With the agreement between the experimental data and model predictions, it is concluded that the mass transfer of hydrogen from the gas-liquid interface to the catalyst external surface is rate determining. This indicates a process intensification potential by using packed-bed microreactors to improve gas-liquid-solid mass transfer. Cold-flow testing of an empty capillary microreactor (inner diameter: 1.6 mm; length: 0.3 m) was initiated and its potential for enhancing the performance of LA hydrogenation to GVL was discussed.

Contents

Abstract	2
Acknowledgements	5
Notation	6
1 Introduction	7
1.1 Biomass valorisation	7
1.2 Levulinic acid hydrogenation to γ -valerolactone	7
1.3 State of the art for levulinic acid hydrogenation	9
1.4 Continuous flow reactors	11
1.4.1 Trickle bed reactors	11
1.4.2 Microreactors	12
1.5 Objective	12
1.6 Research question	12
1.7 Approach	13
2 Theory	13
2.1 Flow regimes	13
2.1.1 Trickle flow regime	14
2.1.2 Pulse flow regime	14
2.1.3 Spray flow regime	15
2.1.4 Bubbling flow regime	15
2.1.5 Slug flow regime	15
2.2 Mass transfer limitations	15
2.2.1 Absorption of gas to the gas-liquid interface	17
2.2.2 Diffusion from the gas-liquid interface to the bulk of the liquid	17
2.2.3 Diffusion from the bulk of the liquid to the external surface of the catalyst	17
2.2.4 Internal diffusion of the reactant in the catalyst pores and reaction	17
2.3 Deriving the overall reaction rate	18
3 Experimental	19
3.1 Reaction test in mini-scale packed-bed reactor	19
3.2 Data analysis with NMR spectroscopy	21
3.3 Experimental overview	21
3.4 Flow regime prediction	24
3.5 Deriving a plot for mass transfer limitations	26
3.6 Catalyst particle size analysis	27

3.7	Microreactor setup	27
3.8	Flow pattern dependency on pressure in the microreactor	29
4	Results & Discussion	29
4.1	Experiments	29
4.1.1	Conversion vs. catalyst loading	31
4.1.2	Reproducibility of experiments	32
4.1.3	Variations in flow ratio	32
4.2	Kinetic model analysis	32
4.2.1	Gas-liquid resistance	33
4.2.2	Liquid-solid resistance	33
4.2.3	Kinetic resistance	33
4.2.4	Mass transfer limitations	34
4.2.5	Model Temperature dependency	35
4.2.6	Model effectiveness factor dependency	37
4.2.7	Model coarse vs. fine catalyst	37
4.2.8	Estimation of $k_i a_i$	38
4.3	Microreactor	39
4.3.1	Setup testing	39
4.3.2	Flow pattern dependency on pressure	40
4.4	Particle size distribution	41
4.5	Reproducibility	41
4.5.1	Catalyst mixing	41
4.5.2	NMR analysis considerations	42
4.5.3	Residence time variations	42
4.6	Catalyst deactivation	42
4.7	Catalyst recycling	43
4.8	Catalyst particle size distribution	43
4.9	Scale up	43
5	Conclusion	43
6	Recommendations for future research	44
7	Bibliography	45
8	Appendix	48
8.1	Experimental overview:	48
8.2	Values for used parameters	50
8.3	Flow pattern dependency on pressure	50
8.4	Particle analysis	53

Acknowledgements

First of all I would like to sincerely thank Jun Yue and Arne Hommes. Jun for always making time for our weekly meeting and helping me to shape the project and the support in setting the goals to be able to finish the project in time. Arne for always having an open door and ear as well as asking the right questions at the right time. I would like to thank Prof. Erik Heeres for his invaluable insights on the project, after each meeting with Erik the project was accelerated forward.

I would like to thank Erwin Wilbers for helping me get started with the reactor and showing me around the analytical process and for always being there to provide technical assistance. I would like to thank Henk van de Bovenkamp for helping me with troubleshooting in both the equipment as well as in the data analysis. Also thanks to Anne Appeldoorn and Marcel de Vries for their assistance in building up the reactor setup and for their technical input on the microreactor.

I would like to thank the people with whom I shared my office (Rianne, Dian, Fenna, Ali, Wouter-Jan) for all the good times we had in and around the office. As well as everybody from the department with whom I shared numerous coffee- and lunch breaks.

And last but certainly not least I would like to thank Maloes, without her gentle coercion and loving support I would not have been able to make it.

Notation

a_c	= Specific surface area of catalyst particle, based on catalyst weight (m^2/g)
a_i	= Gas-liquid interfacial area, based on reactor volume (m^2/m^3)
$C_A(g)$	= Bulk gas phase concentration of A, (mol/m^3)
$C_{A,b}$	= Concentration of hydrogen in the liquid bulk (mol/m^3)
$C_{A,i}$	= Concentration of hydrogen in the liquid at the gas-liquid interface (mol/m^3)
$C_{A,s}$	= Concentration of hydrogen on the catalyst external surface (mol/m^3)
$C_{B,s}$	= Concentration of levulinic acid on the catalyst external surface (mol/m^3)
d_p	= Diameter of catalyst particle (m)
D	= Inner diameter of reactor (m)
\mathbb{D}	= Diffusivity (m^2/s)
G_x	= Superficial mass velocity of phase X ($\text{kg}/[\text{m}^2 \cdot \text{s}]$)
H	= Henry constant of hydrogen in water (-)
k	= Overall mass transfer coefficient for gas into the pellet ($\text{mol}/[\text{g} \cdot \text{s}]$)
k_c	= Liquid-solid mass transfer coefficient (m/s)
k_l	= Liquid phase mass transfer coefficient (m/s)
k_g	= Gas phase mass transfer coefficient (m/s)
R_A	= Overall rate of reaction of A (mol/s)
$-r'_A$	= Rate of disappearance of A per mass of catalyst ($\text{mol}/[\text{g} \cdot \text{s}]$)
Re	= Reynolds number for phase x (-)
t	= Reaction time (s)
U_x	= Superficial velocity of phase x (m/s)
W	= Catalyst weight (g)

Greek symbols

ϵ_b	= Packed bed porosity (-)
η	= Internal effectiveness factor (-)
μ_x	= Dynamic viscosity of the fluid (x is either gas or liquid) ($\text{kg}/[\text{m} \cdot \text{s}]$)
ρ_x	= Density of catalyst pellet (kg/m^3)
τ	= Residence time (s)
\emptyset_V	= Volumetric flow rate (m^3/s)

Subscript

G	= Gas phase
L	= Liquid phase
P	= Catalyst particle

1 Introduction

1.1 Biomass valorisation

In order to facilitate the transition from fossil fuels and chemicals derived thereof to renewable resources, there is an increasing interest for the valorisation of biomass feedstocks. Biomass-based routes will increase their share in the total bulk chemical production [1]. Lignocellulosic biomass is an abundant source of renewables that can be used to replace fossil resources in both chemicals and fuels. The conversion of biomass into platform chemicals with a broad application range could well be used to address increasing environmental concerns such as climate change and the depletion of fossil fuel resources. Platform chemicals can be defined as: chemicals that serve as a platform for the synthesis of numerous bulk chemicals [2]. These platform chemicals include, among others, glycerol, glutamic acid, aspartic acid and levulinic acid [1].

A promising strategy for biomass conversion into platform chemicals is by the conversion of lignocellulose-derived sugars to levulinic acid (LA) [3]. LA can be obtained simply and with high yield by the dehydration of C6-sugars in acidic media through hydroxymethylfurfural as intermediate. LA can be converted to substituted pyrrolidones, lactones and levulinate esters [1].

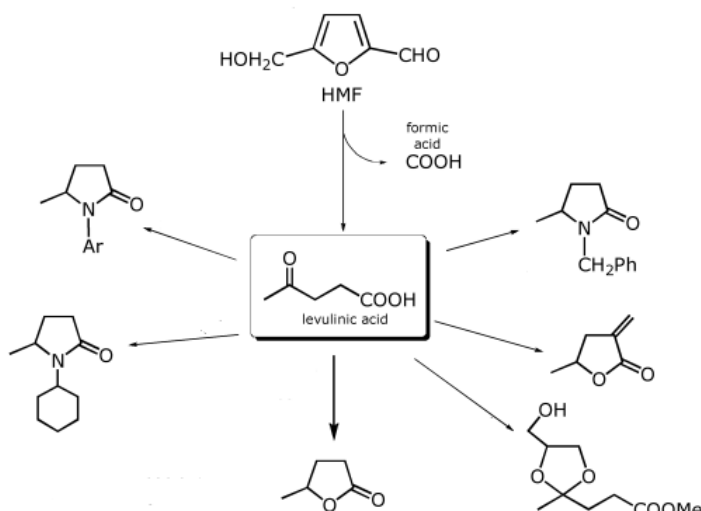


Figure 1, levulinic acid as a precursor for bulk chemical [1].

One of the possible products that can be made from LA is γ -valerolactone (GVL), as shown in the centre-bottom in Figure 1. GVL is itself also a platform chemical. It has a recognisable but acceptable scent, which makes it easy to identify leaks in processing. It is non-toxic, water soluble, biodegradable and widely used as a food additive. GVL can serve as: a renewable feed for chemicals like solvents and bulk chemicals (e.g. methylpentenoates and adipic acid); as an intermediate in chemicals synthesis and for fuel (additives). GVL has gained increasing interest because of its versatile functions and because of its lack of hazardous properties. It can be converted to monomers for the production of nylon and high thermal stability polymers [4].

1.2 Levulinic acid hydrogenation to γ -valerolactone

Figure 2 gives a reaction mechanism for the formation of GVL from LA via hydrogenation. In these proposed mechanisms, LA can be formed either by condensation reaction followed by the hydrogenation or vice versa. In the first reaction mechanism, the intermediate is α -angelicalactone and for the second reaction mechanism, the intermediate is 4-hydroxypentanoic acid. Under different reaction conditions different reaction intermediates were observed [5].

Extensive research has been performed on the hydrogenation of LA to GVL using homogeneous and heterogeneous catalysts.

Homogeneous catalysts used include Ru nanoparticles and Ru with PPh_3 ligands [6] [7]. A disadvantage of using homogeneous catalysts is that after the reaction additional steps are required to separate the product from the reaction mixture [8].

The heterogeneous catalysts include Ir, Rh, Pd, Ru, Pt, Re and Ni supported on activated carbon or other supports. These studies focus on either continuous or batch mode liquid phase reaction. Many studies report high LA conversion (up to 100%) and high selectivity to GVL (>90%) [4] [5] [9] [10] [11] [12]. It was found that among heterogeneous catalysts investigated so far, ruthenium has the highest activity and selectivity for GVL synthesis [13]. In previous work in this research group, it was found that the intermediate 4-hydroxypentanoic acid (4-HPA) was present in small quantities in the product stream. [5] The intermediate is spontaneously hydrolysed to GVL. The intermediate α -angelicalactone (α -AL) was not found under the prevailing reaction conditions. Also at higher temperatures subsequent hydrogenation of GVL was not observed [5]. Some studies investigated the deactivation of Ru/C under reaction conditions. After 100 hours on stream the loss of activity has been found to be in the order of 0.2 % per hour [5] [9] [13].

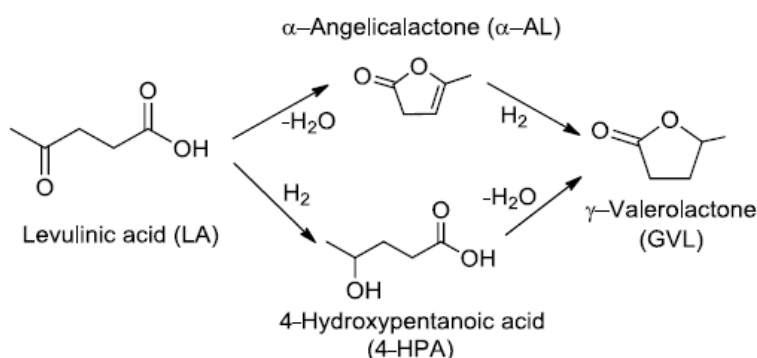


Figure 2, possible reaction pathway for GVL synthesis [5].

The hydrogenation of LA can also be achieved using an acid to donate the hydrogen instead of molecular hydrogen. A study reported on the hydrogenation using formic acid as a hydrogen source without using a hydrogen gas phase. At a temperature of 150 °C and using NEt_3 as a base with PPh_3 ligands the GVL yield from LA can be as high as 90%. Other ligands and bases were also tested, but have been found to have lower yields [5] [13] [14].

Much research into the hydrogenation of LA into GVL has been done, as shown in Table 1. Many of the batch studies operate at high temperature ($T = 340 - 470 \text{ K}$) and use long reaction times ($> 6 \text{ hrs}$) to reach high conversion of LA. For continuous setup, the temperature is generally lower ($T = 275 - 420 \text{ K}$).

Limited research has been done to determine the rate limiting contributions to the reaction, other than the intrinsic kinetics. Two studies reported that the hydrogenation reaction is 0th-order in LA and 0.5th-order in H₂ [11] [13]. For modelling purposes these kinetics will also be used in this study. One study did report that the rate of reaction is mostly independent of the catalyst loading [5]. This implies that the reaction is not kinetically limited, which is an indication that the mass transfer limitations are dominating. In general for liquid-phase hydrogenation, it is highly likely that the reaction can be rate limited by mass transfer, particularly mass transfer from gas to liquid and/or liquid to solid. This depends on many parameters such as catalyst particle size, gas-liquid interface surface and the reactor setup.

1.3 State of the art for levulinic acid hydrogenation

Catalyst	Reaction conditions	Reactor type	Conclusion	Reference
Heterogeneous catalysed hydrogenation of LA to GVL with 0.5 wt% Ru/C	$T = 343 - 403 \text{ K};$ $p = 30 - 60 \text{ bar};$ $LA_{in} = 0.3 - 2.5 \text{ M},$ $t = 4\ 320 \text{ hours}.$	Batch slurry bed experiments and kinetic modelling (Langmuir-Hinshelwood approach)	Intra-particle diffusion affects the overall reaction rate, mass transfer and diffusion limitations not taken into account	[13]
Heterogeneous catalysed hydrogenation of LA to GVL over supported 15 wt%. nickel catalysts (Ni/Al₂O₃-incipient wet impregnated and Ni/Al₂O₃-wet impregnated)	$T = 393 - 473 \text{ K};$ $p = 10 - 50 \text{ bar};$ $t = 7\ 200 \text{ s};$ Solvents: monovalent alcohols (C ₁ – C ₅), acetic acid, DMF and water.	Catalyst preparation and characterisation with catalyst testing in batch autoclaves.	Using alcohols as solvents leads to side reactions that can be suppressed by raising the hydrogen pressure ($p > 20 \text{ bar}$). When no solvent are present, high yield and selectivity for GVL were obtained (92% and 100% respectively). Significant catalyst deactivation was observed.	[8]
Homogeneous hydrogenation of LA to GVL with Ru(acac)₃ and RuCl₃ using phosphine ligands.	$T = 473 \text{ K};$ $p = 50 \text{ bar};$ stirring rate = 1400 rpm; $t = 86\ 400 \text{ s}.$	Batch slurry bed reactor	More bulky ligands increased observed conversion. Phosphine ligands gave the best catalytic result (94-99 % conversion after 5 hours).	[7]
Homogeneous transfer hydrogenation of LA with different bases. Using RuCl₃ and PPh₃ as the catalyst.	$T = 373 - 473 \text{ K};$ $p = 1 \text{ bar};$ high LA concentration; $t = 21\ 600 \text{ s};$	Batch slurry bed reactor	At a temperature of 423 K and using NEt ₃ as a base with PPh ₃ ligands the GVL yield from LA can be as high as 90% in 6 hours. Adding CO ₂ can greatly increase the yield of GVL.	[14]
Homogeneous hydrogenation of LA to GVL using	$T = 388 - 403 \text{ K};$ $p = 0 - 35 \text{ bar};$ $d_p < 5 \text{ nm};$	In-situ catalyst preparation and	High yields for GVL are reached (up to 100 %) both for transfer hydrogenation	[6]

Ru nanoparticles. Using either molecular hydrogen or formic acid.	$t = 6 - 42$ hours; $C_{LA,in,1} = 86 \cdot 10^{-3}$ M; $C_{LA,in,2} = 1.2$ M.	batch reaction in autoclave.	and molecular hydrogen. Initial catalyst recycling was successful but later	
Vapor phase hydrogenation of aqueous LA over HAP supported metal (M= Pd, Pt, Ru, Cu, Ni) catalysts	$T = 275 - 375$ K; $p = 1$ bar; $d_p = 3-8$ nm; $\tau =$ unspecified.	Continuous packed bed reactor	Ru/HAP showed higher TOF and selectivity for GVL than the other metal catalysts. Adding SO_4^{2-} changes the selectivity of the catalyst from the hydrogenation towards α -angelica lactone	[12]
Heterogeneous hydrogenation of LA to GVL over Ru/C, Pt/C and Pd/C.	$W = 1$ g; $T = 538$ K; $p = 1 - 25$ bar; $\tau = 7\ 020$ s.	Continuous down flow packed bed reactor	In the hydrogenation of 5 wt%. Ru/C was shown to have 100 % conversion and selectivity towards GVL for up to 24 hours on stream. The higher stability of Ru/C over Pt/C and Pd/C was attributed to the higher dispersion degree of Ru compared to Pt and Pd.	[10]
Heterogeneous catalysed hydrogenation of LA to GVL with Ru/C, Ru/Al₂O₃ and RuTiO₂	$T = 363$ K; $LA_{in} = 1.2$ M; $H_{2,in} = 30$ ml/min; $\tau = 180$ s.	Continuous packed bed reactor	Intraparticle diffusion confirmed by experiments with different catalyst particle sizes. Ru/C had higher stability and activity compared to Ru/Al ₂ O ₃ and RuTiO ₂ . Catalyst specific surface area of the catalyst significantly decreased and sintering of Ru was observed	[5]
Heterogeneous catalysed hydrogenation of LA to GVL with 5 wt% Ru/C	$T = 323 - 423$ K; $p = 4.1 - 41.5$ bar; $d_p = 45-90$ nm; $LA_{in} = 0.025- 1.5$ M; $\tau = 6.5 - 72$ s.	Continuous packed bed reactor and kinetic modelling	For $T < 423$ K the reaction pathway proceeds exclusively via the HPA intermediate. Apparent E_A values for LA hydrogenation to and subsequent esterification of 4-HPA are 48 and 70 kJ mol ⁻¹ , respectively.	[11]

Homogeneous hydrogenation of LA to GVL using PNP-Ir pincer complexes.	$T = 298 \text{ K};$ $p = 1 \text{ bar};$ $\tau = \text{unspecified.}$	Computational study	The hydride transfer step has a significantly higher activation energy than the methylene proton transfer. Therefore hydride transfer is the rate-limiting step.	[15]
--	--	---------------------	--	------

Table 1, state of the art of LA hydrogenation to GVL.

1.4 Continuous flow reactors

For large scale industrial processes continuous reactors are used instead of batch processes to ensure constant product quality and production rate. In this chapter two examples of continuous reactors are discussed that have been used or could be used for the hydrogenation of LA to GVL.

1.4.1 Trickle bed reactors

Trickle bed reactors as gas-liquid-solid contacting devices are a useful tool for multiphase reactions [16]. The reactors are useful for industrial large volume processing. In trickle bed reactors a gas phase and a liquid phase flow over a bed of solid catalyst particles [16]. A few examples of the ways in which trickle bed reactors can be operated are shown in Figure 3. These flows can be co-current or counter-current. The direction of the flow is often downwards to utilize the gravitational pull, but can also be operated in an upward direction. The name of the reactor, trickle bed, describes the flow regime of its operational characteristics where the liquid that flows over the catalyst surface forms a film, droplets or rivulets.

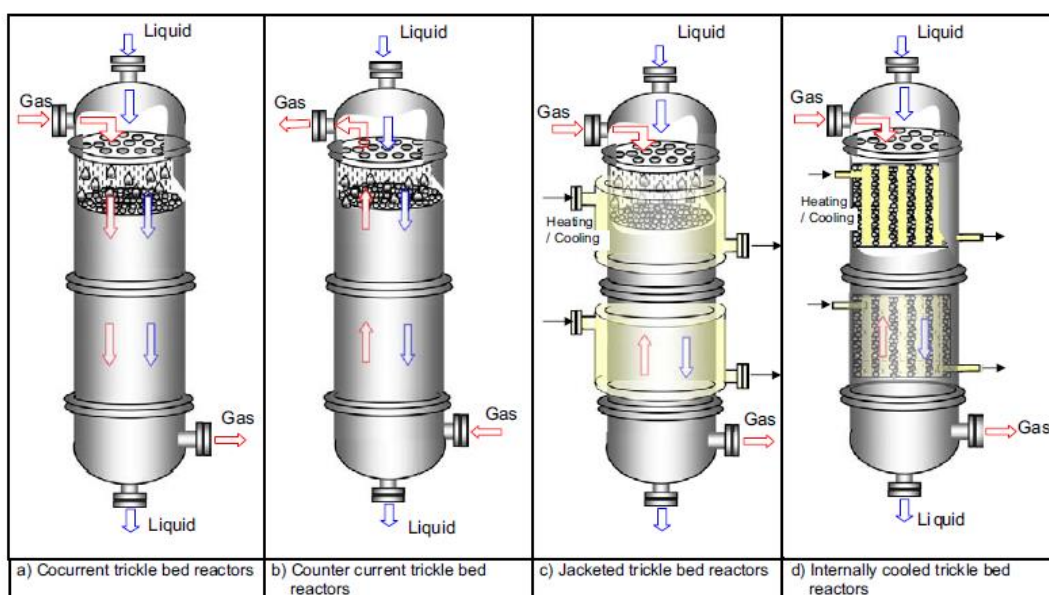


Figure 3, various configurations of trickle bed reactors [16].

The performance of a trickle bed reactor depends on several parameters such as: catalytic bed characteristics (porosity, particle size, packing configuration), flow (mal-)distribution, catalyst particle wetting, heat distribution, mass transfer rates, intra-particle mass, heat transfer and kinetics of the reaction [16].

1.4.2 Microreactors

Continuous flow microreactors can be considered as a plug flow reactor with a typical inner diameter of 0.1 – 1 mm. Microreactors offer excellent mass and heat transfer performance for multiphase reactions. In the tiny micro channels, the gas-liquid mixture has more interfacial area per liquid volume (on the order of 10,000 m²/m³) which is an advantage for accelerated mass transfer [17]. Increasing the gas-liquid interfacial area will improve the gas-liquid mass transfer. Another way in which microreactors can help improve the rate of reaction is by allowing the use of even smaller catalyst particles. Using finer particles increases the specific catalyst surface. In large reactors the particle size used has a lower limit because using too fine a powder requires more care in handling. Microreactors can also ensure a tight reaction temperature control which is often crucial for obtaining a high product selectivity [18].

Understanding the limitations of the process is necessary for improved yields of the desired products. In a microreactor the catalyst can be inserted in 3 ways: coating the catalyst on the channel walls; using a homogeneous catalyst that flows through the reactor with the reactants, and the third method is using a catalytic packed-bed microreactor. Of these 3 methods of catalyst insertion, the easiest method is to use random packing as it needs no special coating steps and doesn't require a separation step to remove the catalyst from the product stream.

In a study from 2005 it is stated that "... micro fixed beds are rarely used..." [19]. However since 2005 the publications on microreactor packed bed reactors have seen an increase. This shows that the academic interest in packed-bed microreactors has been growing in the last decade.

Using small particle size ($0.05 < d_p < 0.2$ mm) in a packed-bed microreactor can lead to extensive gas bypassing. This is due to capillary forces dominating over gravitational forces [20]. So far, there is no report in LA hydrogenation in packed-bed microreactors.

1.5 Objective

The problem under investigation is two-fold. First is the problem of mass transfer limitations in the production of bio based platform chemicals such as GVL. Finding ways to reduce these limitations will help to make the large scale production of bio-based chemicals more efficient. This in turn will aid in the transition from fossil fuel-based chemicals to bio-based chemicals.

The second part of the problem is the limited knowledge of microreactor technology. This study is also aimed to provide the basis for improved mass transfer in a packed-bed microreactor, especially in relation to LA hydrogenation to GVL.

1.6 Research question

This study is aimed at investigating mass transfer in comparison with the reaction kinetics for the hydrogenation of levulinic acid to γ -valerolactone using heterogeneous ruthenium on carbon catalyst in continuous reactors (i.e., mini-scale packed-reactor and microreactor). The effects of temperature, flow

rate, catalyst weight on LA conversion and product yield are evaluated. Initial testing showed that the concentration of the intermediate 4-HPA was very small compared to the concentration of LA and GVL. A mathematic model was derived based on an equation derived to distinguish between gas adsorption limitations and kinetical limitations.

The main research question for this thesis is:

Is mass transfer from the gas to the catalyst determining the rate of hydrogenation of levulinic acid to γ -valerolactone, and if so, can a microreactor help improve the reaction rate?

1.7 Approach

To investigate the different resistance contributions to the overall reaction rate, the overall rate equation is derived. A set of experiments is designed to determine the rate of reaction for different catalyst packing weights. Using the experimental data the validity of a model based on the overall reaction rate is evaluated. The model is used to make predictions on the contributions of different resistances, the outcome of which will indicate the intensification potential of microreactors.

2 Theory

2.1 Flow regimes

When fluids flow through a network of porous pellets the fluids will preferably flow through the path of the least resistance. This can result in inhomogeneous velocities, phase transitions and channel formation. Different flow regimes are observed even in single-phase flows through packed beds. Within a packed bed several different types of flow regimes can occur, based on parameters such as: gas flow rate, liquid flow rate, particle size and bed diameter. The literature differentiates between 5 regimes, these are: trickle flow; pulse flow; spray, bubbly and slug flow. The first of these 4 flow regimes are shown in Figure 4. There have been many studies in literature proposing models to predict the flow regime of packed-bed reactors and bubble columns [16] [21] [22] [23] [24] [25]. For a single-phase reactor, the flow regime can be predicted relatively easy, but in a reactor with a multiphase flow the situation is more complex. In this study, the reactor is operated with cocurrent gas and liquid flow. Flow characteristics of these regimes are quite distinct and therefore it is important to make an accurate prediction of the flow pattern. When comparing performance of two reactor types (e.g. microreactor vs. small scale reactor), the flow characteristics are a key consideration. The models discussed all have limited range of applicability, therefore it is important to choose the most applicable model to allow for an accurate prediction.

The different flow regimes described above can have a strong effect on the mass transfer (as well as heat or momentum transfer). This is because the interfacial area between gas and liquid differs greatly between different flow regimes [23].

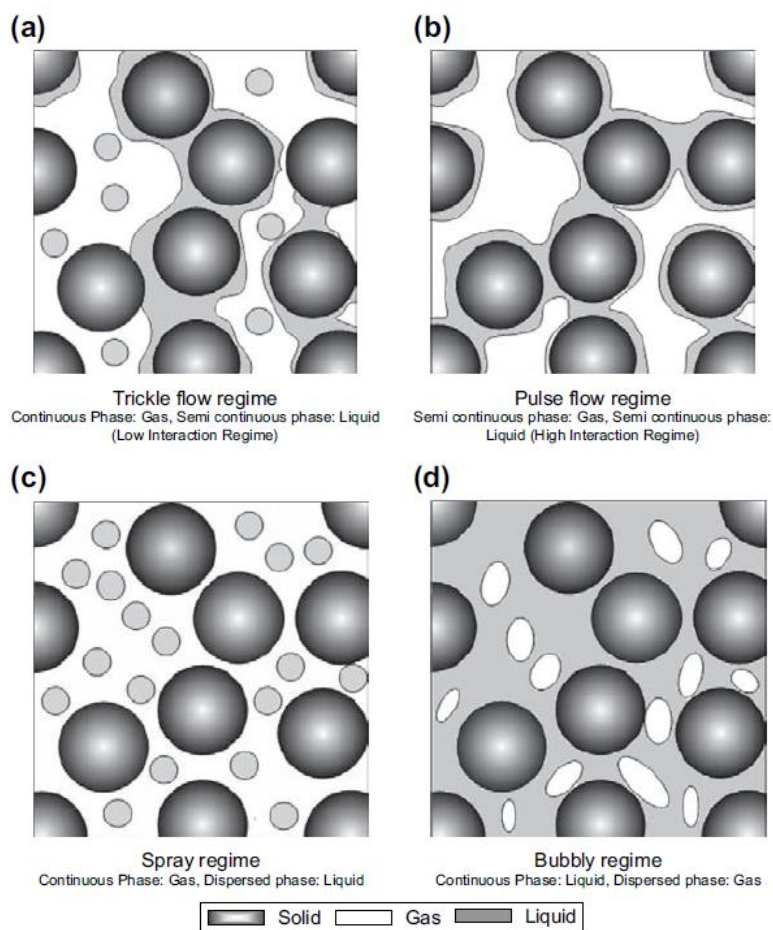


Figure 4, flow regimes in trickle bed reactors [16] [23].

2.1.1 Trickle flow regime

Trickle flow occurs when the liquid flow rate is low and the gas flow rate is moderate. The liquid flows over the catalyst particles in rivulets or films. Because of the low liquid flow rates, the inertial forces are weak compared to the surface forces. At higher flow rates, the inertial forces will be strong compared to the surface forces, which results in film formation. Trickle flows occur up to a liquid flow rate of 12-15 kg/(m²s) and a gas flow rate of 1.25 kg/(m²s). How much a liquid is prone to foaming can significantly affect the boundaries of the trickle flow regime. Trickle flow regime region shrinks with decreasing particle size, increasing liquid viscosity and increasing surface tension [16].

2.1.2 Pulse flow regime

When either the gas flow rate or the liquid flow rate is increased there is a transition from the trickle flow regime into the pulse flow regime. In the pulse flow regime, the gas phase flow is locally blocked by the liquid flow. This results in the formation of alternating gas and liquid zones. In the liquid enriched zones, complete wetting of particles occurs. The boundaries of pulse flow are significantly affected by the foaming properties of the liquid. For liquids that are not prone to foaming, the alternating zones are distinct and visible, and there is a tendency for a transition from the pulse flow regime into the bubbly flow regime. Many industrial trickle bed reactors are operated in the boundary layer between pulse flow and trickle flow regime to take advantage of both regimes [16].

2.1.3 Spray flow regime

When operating at high gas flow rate and low liquid flow rate, the liquid flow can loosen into a semi-continuous flow or even be spread into droplets. This is caused by the shear forces the high flow rate of the gas exerts on the liquid phase. This regime is called the spray flow regime. The boundary between the trickle flow regime and spray flow regime can be difficult to identify. This regime occurs typically up to a liquid flow rate of $12 \text{ kg}/(\text{m}^2\text{s})$ and gas flow rates higher than $1.25 \text{ kg}/(\text{m}^2\text{s})$. This regime has the advantages of a low liquid holdup, high gas-liquid mass transfer rates and low foaming [16].

2.1.4 Bubbling flow regime

At high liquid flow rate and low gas flow rate, the liquid forms a continuous phase between the gaps of the particles. The gas phase flows through the liquid phase in the form of bubbles, hence the name bubbling flow. The advantages of this regime are that the particles are completely wetted and there is a high heat and mass transfer rate. This regime is useful for reactions where the liquid phase transport is limiting or the case where the reaction is highly exothermic. A disadvantage of this regime is that there can be higher liquid holdup that leads to back mixing [16].

2.1.5 Slug flow regime

The slug flow regime is commonly observed in microreactors. This flow pattern can be achieved by using a 'T'- or 'Y'-junction to mix the reaction streams. In slug flow, gas bubbles are separated by liquid. Any catalyst particle exposed to slug flow will alternately be exposed to gas and liquid. The main advantage of slug flow is that within the slug the fluid circulates which improves the mixing of the fluid. This improves the mass transfer rate both at the gas-liquid interface and the diffusion through the liquid [26] [27].

2.2 Mass transfer limitations

Multiphase catalytic reactions play important roles, not only in the research laboratory, but also in the chemical and pharmaceutical industries. They are classified according to the phases involved, such as gas-liquid, gas-liquid-liquid, or gas-liquid-solid reactions. Although numerous multiphase catalytic reactions are known and used in industry, these reactions are still difficult to conduct when compared to homogeneous reactions, because the efficiency of interaction and mass transfer between different phases tends to be low, and thus in most cases the reaction rates are slow. [5] [10]. Increasing the understanding of the limitations of the process will help improve the yields of the desired products [28].

In a continuous multiphase reactor, there are a number of steps the gas phase has to pass through before it can react on the catalyst surface. When the reaction has reached steady state, the slowest of the 5 steps outlined below will determine the overall reaction rate. These steps correspond to the steps shown in Figure 5 and 6.

1. Absorption from the gas phase to the gas-liquid interface;
2. Diffusion (molecular and/or convective) from the gas-liquid interface to the bulk of the liquid;
3. Diffusion (molecular and/or convective) from the bulk of the liquid to the external surface of the catalyst;
4. Internal diffusion of the reactant within the catalyst pores;

5. Reaction at the catalyst surface.

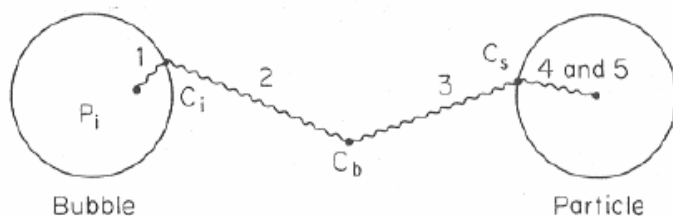


Figure 5, schematic representation of the mass transfer steps for the gas phase component [29].

Liquid-phase hydrogenation of levulinic acid to γ -valerolactone over solid catalysts (e.g, Ru/C) also undergoes these steps. But for levulinic acid, because it is already in the liquid phase the first 2 steps do not occur (i.e., steps 1-5 are for hydrogen). The rate determining step can be found by measuring the rate of disappearance of the reactant for each of these steps. Since the rate determining step will determine the overall rate of reaction, the pseudo steady state of the component can be assumed. This means that the time derivative of the component is constant for every step and that the reaction rate (R_A) is the same for each step. The method used here to derive is analogous for the method of deriving an overall rate equation for a slurry reactor [29]. The values and the derivation for the parameters used in the equations below can be found in Appendix 8.2.

A number of studies show that the Ru/C heterogeneously catalysed hydrogenation of LA to GVL is limited by mass transfer [5] [13].

Mass transfer is limiting if the reaction rate is relatively fast compared to the mass transfer. This occurs if hydrogen reacts with LA faster than it is transferred to the catalyst surface. As shown in Figure 6 the concentration of gas in the gas phase (left) is higher and decreases as it approaches the gas-liquid interface. At the gas-liquid interface the gas is absorbed into the liquid. Less gas can be dissolved in the liquid phase than in the gas phase. Within the liquid the dissolved gas concentration is highest at the gas liquid interface, and decreases with distance from the interface. At the liquid solid interface the gas can diffuse to the catalyst surface and react. This results in a sharp decrease in the concentration of dissolved gas in the liquid.

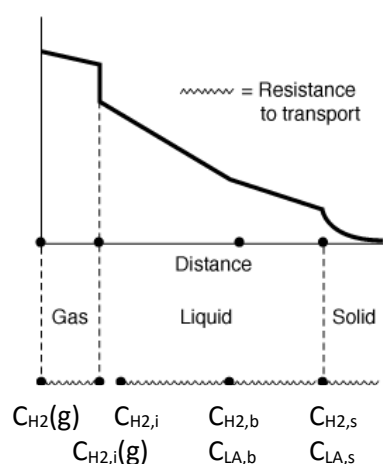


Figure 6, concentration profile for gas phase component from gas to liquid [30].

2.2.1 Absorption of gas to the gas-liquid interface

$$R_{H_2} = \frac{k_g a_i H W}{(1 - \epsilon_b)\rho_p} \left[\frac{C_{H_2}(g)}{H} - C_{H_2,i} \right]$$

Equation 1

Equation 1 describes the diffusion of the gas through the gas-liquid interface. a_i is the gas-liquid interfacial area based on the reactor volume. Equation 1 is neglected in this study because the hydrogen concentration is constant between the gas bulk and the gas-liquid interface. This is valid because pure hydrogen gas is used instead of a gas mixture (as will be detailed in Chapter 3).

The Henry constant for hydrogen in water is used to determine the concentration of hydrogen at the liquid side of the gas-liquid interface. This is shown in Equation 2 in which H is the Henry constant defined in mass of gas dissolved per mass of liquid.

$$C_{H_2}(g) = H C_{H_2,i}$$

Equation 2

2.2.2 Diffusion from the gas-liquid interface to the bulk of the liquid

$$R_{H_2} = \frac{W k_l a_i}{(1 - \epsilon_b)\rho_p} [C_{H_2,i} - C_{H_2,b}]$$

Equation 3

$$R_{H_2} = V k_l a_i [C_{H_2,i} - C_{H_2,b}]$$

Equation 4

Equation 3 describes the diffusion of component A from the gas liquid interface to the liquid bulk.

Equation 3 is simplified by using $\frac{W}{(1-\epsilon_b)\rho_p} = V$, which yields Equation 4. Also the gas concentration at the gas side of the gas-liquid interface is equal to the gas concentration in the gas bulk, which follows from using only pure hydrogen.

2.2.3 Diffusion from the bulk of the liquid to the external surface of the catalyst

$$R_{H_2} = W (k_c a_c) [C_{H_2,b} - C_{H_2,s}]$$

Equation 5

Equation 5 describes the rate of hydrogen travelling from the bulk liquid to the catalyst external surface, where $k_c a_c$ is the mass transfer rate of hydrogen through water multiplied by the catalyst surface area per catalyst weight.

2.2.4 Internal diffusion of the reactant in the catalyst pores and reaction

$$R_{H_2} = W \eta k \sqrt{C_{H_2,s}}$$

Equation 6

$$\left(\frac{R_{H_2}}{W \eta k}\right)^2 = C_{H_2,s}$$

Equation 7

In literature the hydrogenation of LA is found to be ½th order in hydrogen and 0th order in LA [11] [13]. The rate of reaction is shown in Equation 6 where k is the intrinsic rate of reaction which can be derived using the Arrhenius equation [11] [13].

By taking the square of Equation 6 and rearranging the equation, the concentration of hydrogen on the catalyst surface ($C_{A,s}$) can be isolated as shown in Equation 7.

2.3 Deriving the overall reaction rate

Rearranging and adding up Equation 2, 4, 5 and 7 yields Equation 8. The concentration of hydrogen in the bulk and the hydrogen concentration on the catalyst surface are eliminated from the equation.

$$\frac{C_{H_2}(g)}{R_{H_2}} = \frac{H}{V k_l a_i} + \left(\frac{H}{W} \frac{1}{k_c a_c} + \frac{H}{W^2} \frac{R_{H_2}}{(\eta k)^2}\right)$$

Equation 8

To isolate R_A from Equation 8 the variables are rearranged to the form of Equation 9 which is a quadratic equation

$$0 = R_{H_2}^2 \frac{H}{(W \eta k)^2} + R_{H_2} \left(\frac{H}{W} \frac{1}{k_c a_c} + \frac{H}{V k_l a_i} \right) - C_{H_2}(g)$$

Equation 9

Solving Equation 9 for R_A yields Equation 10, which can be used to calculate the value for R_A .

$$R_{H_2} = \frac{-\left(\frac{H}{V k_l a_i} + \frac{H}{W} \frac{1}{k_c a_c}\right) + \sqrt{\left(\frac{H}{V k_l a_i} + \frac{H}{W} \frac{1}{k_c a_c}\right)^2 + \frac{4 H C_{H_2}(g)}{(W \eta k)^2}}}{\frac{2 H}{(W \eta k)^2}}$$

Equation 10

3 Experimental

In this study a series of experiments were performed to determine whether the reaction is limited by mass transfer from gas to liquid or from diffusion through the liquid and catalyst.

3.1 Reaction test in mini-scale packed-bed reactor

The setup for the mini scale reactor is schematically shown in Figure 7. In Figure 8 a photograph of the small reactor setup is shown.

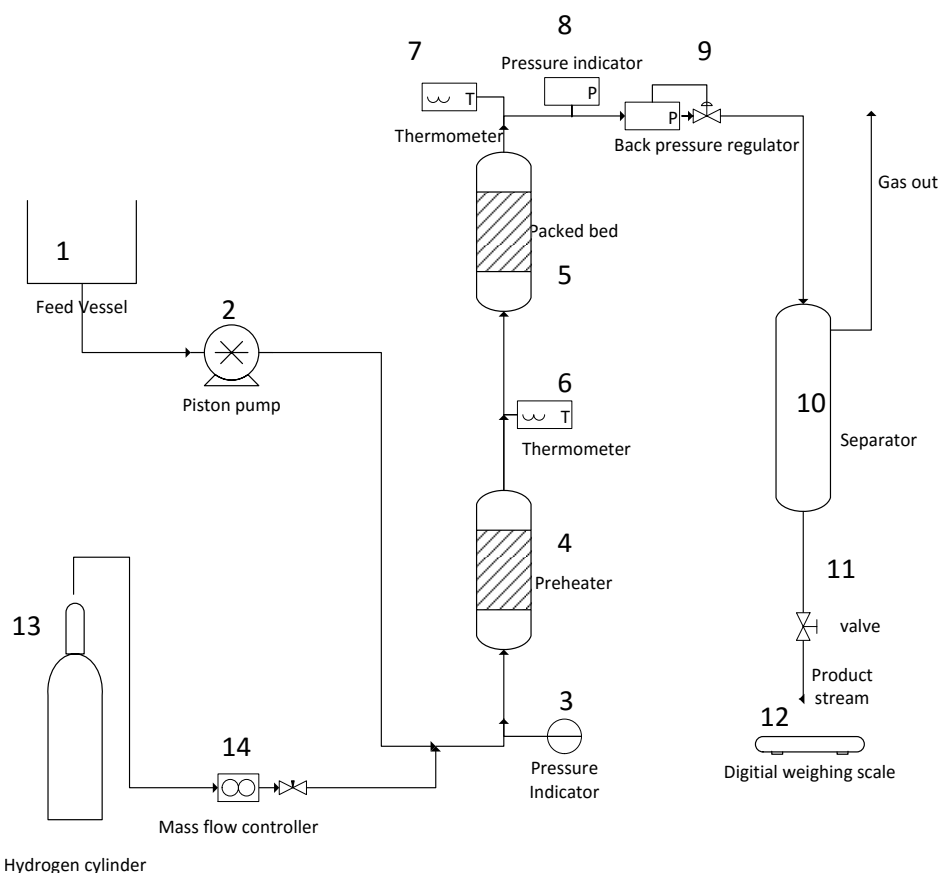


Figure 7, PFD for mini-scale packed bed reactor setup.

A levulinic acid solution is made by mixing 142.3 gram of >98% pure levulinic acid, purchased from Acros Organics, and adding Milli-Q water to a total of 1 liter, the LA concentration of the solution being 1.2 mol/L. The solution is fed to the reactor by an air driven pump (MARK XIIA Oscillamatic by Williams Milton Roy) to achieve a liquid flow rate of 1 mL/min. Hydrogen gas from a cylinder is passed through a reducer to reduce the pressure to 50 bar, a mass flow controller is placed downstream from the reducer to regulate the mass flow of H₂ to the reactor. The mass flow controller (Bronkhorst HI-TEC type: F-201C-Fa-22-V) shows the volumetric flow rate under normal condition (1 atm, 0 °C). The actual volumetric flow rate is corrected for temperature and pressure using the ideal gas law given as shown in Equation 11.

$$\phi_{V,actual} = \phi_{V,0} \frac{p_0}{p_{actual}} \frac{T_{actual}}{T_0}$$

Equation 11

A one-way valve is inserted after the mass flow regulator to prevent back-flow of liquid. The gas and the LA solution are mixed and passed through a preheating section. In the preheating section the mixture is heated to 90 °C. The gas-liquid mixture then enters the reactor, a 4 mL tube, which is filled with a packed bed of catalysts. 0.5% Ru/C was purchased from STREM. The catalyst particles were crushed and sieved to a particle size of $1.25 \text{ mm} < d_p < 2.5 \text{ mm}$ (coarse) and $0.5 \text{ mm} < d_p < 1.25 \text{ mm}$ (fine).

The residence time at the benchmark conditions is approximately 140 s. The catalyst bed is loaded with catalyst particle or a mixture of catalyst particles and silicon carbide particles of similar particle size. The total mass of the packed bed is around 1.8 g. The compounds are individually weighed in paper cups, then combined and shaken for approximately 20 s to ensure good macroscopic mixing. The powder is then added to the reactor from the top using a small funnel.

The temperature of gas-liquid mixture is measured at the inlet and the outlet of the reactor to ensure the temperature is steady before and during the experiment. The reactor and preheating section are insulated with a layer of glass wool, a layer of cotton strips and a sheet of aluminium. The inlet and outlet of the reactor are fitted with a filter to ensure the catalyst and filler particles remain in the reactor and are not entrained with the fluids and potentially damage the downstream equipment as well as reduce the amount of catalyst available in the reactor. After the reactor, the gas-liquid mixture is guided to a back pressure regulator (Type GBT85-420N100-SSKN spring loaded back pressure regulator by Dutch Regulatos BV). Then, the gas-liquid mixture enters a separator where the gas phase is allowed to escape the separator from the top and the liquid fraction can be extracted with a valve below the separator. The liquid samples that are collected are weighed using a digital scale.

In Figure 8 a photograph of the small scale reactor setup is shown, in the picture numbers show the various elements of the setup as described below. From the liquid feed vessel [1] the liquid flows to the right to the air driven pump [2]. From the pump the liquid is mixed with the gas stream just behind the pressure gauge shown just above the set of spanners [3]. The gas enters the system from a large red cylinder which is just visible in the far right of the picture [12]. The mixture then moves upwards through the preheater [4] and the packed bed [5], which can be identified by the dark coloured heating coils. Between the preheating section and the packed bed [6] and at the top of the packed bed [7] thermometers can be seen protruding out of the reactor with wires relaying the data to a read out (outside of the picture scope). The fluid continues from the packed bed to right, where a pressure meter [8] can be identified by a thick black cable passing the signal to a readout below the setup (outside of the picture scope). The device with the large orange turning cap on top of is the back pressure regulator [9]. The fluid continues down through a separator [10]. The liquid stream is collected from the separator equipped with a valve [11], on to a digital scale [12] used to determine the sample weight.

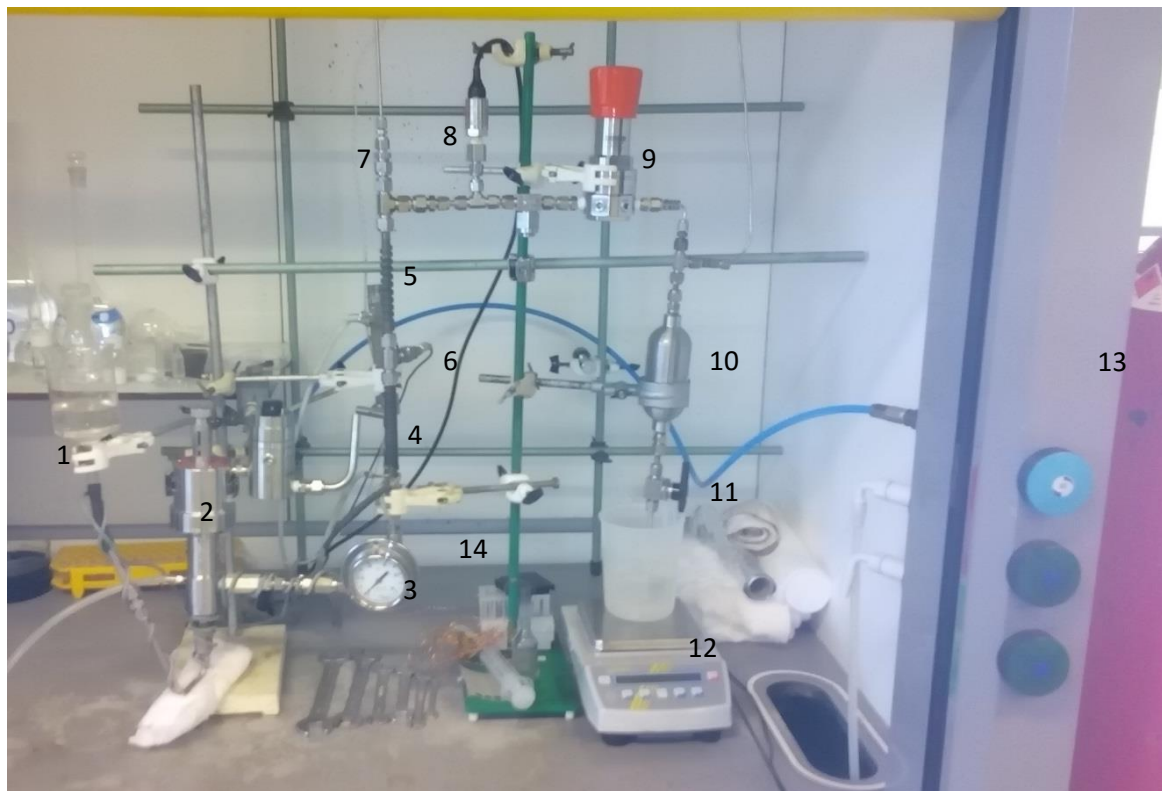


Figure 8, photograph of small reactor setup.

3.2 Data analysis with NMR spectroscopy

The composition of the reaction mixture samples are determined quantitatively by $^1\text{H-NMR}$ to determine the content of LA, HPA and GVL. The samples collected from the reactor small samples are filtered, a NMR tube is filled with a weighed amount of sample. D_2O is added to provide the deuterium to be analysed in the NMR spectrometer. Dioxane is added as an internal standard to determine quantitatively the concentration of LA, HPA and GVL. The samples are placed in a 300 MHz NMR spectrometer, 128 cycles are used. The spectra are analysed using Mestrenova 10.2[®] software. First a phase shift correction and baseline correction are performed. Then the integral of the peaks of the components are calculated using the auto detect function. The accuracy of the AutoDetect function was found to be within 1% of the manual selection procedure. Using Microsoft Office Excel the area of the peaks from the spectra are analysed. The area of the dioxane peak (3.6 ppm), from which the concentration is known, is related to the areas of the peaks corresponding to LA (2.1 ppm). GVL (1.3 ppm) and 4-HPA (1.03 ppm). The inlet concentration of LA is derived from the sum of the concentrations of LA, GVL and 4-HPA. This is used as the total concentration instead of using a measured concentrations at the inlet because using the latter method results in high deviations from a molar balance. No other products from side reactions were observed and this is confirmed by previous research done in the research group. The conversion of LA is calculated to give an indication of the overall reaction performance.

3.3 Experimental overview

The first set of experiments were performed to try and replicate the results achieved in this department [13]. The standard conditions used in all experiments unless stated differently are shown in

Table 2.

Parameter	Value	Units
$C_{LA,in}$	1.2	mol/L
LA feed rate	~1	mL/min
H ₂ feed rate	30	mL/min
Temperature	90	°C
Molar flow rate of H ₂	45	Mmole/min
Hydrogen pressure	45	Bar
WHSV	33	g _{feed} /(g * h)
Run time	3	h
Pellets (large)	1.25-2.5	mm
Pellets (fine)	0.5 -1.25	mm
Catalyst loading (Ruthenium on carbon)	0.5	wt%;

Table 2, standard conditions for small scale experiments.

A complete overview of the experiments done in this study can be found in Table 3, Table 4 and Table 6. Experiments A – E were performed using coarse catalyst particles ($1.25 \text{ mm} < d_p < 2.5 \text{ mm}$). After experiment A and B, the conversion steadies to around 80 %. In experiment D3 the concentration of hydrogen is increased while keeping the volume ratio of gas and liquid in the reactor constant. It can be seen that the conversion increases to 90 %. Experiment E was performed to investigate the large variations in the mole balance. From experiment F and onward all experiments are performed with catalyst that has been ground to a finer powder ($0.5 \text{ mm} < d_p < 1.25 \text{ mm}$).

Experiment	Goal	Conditions
A	Exploratory	Standard, with coarse particle
B	Exploratory	Standard, with coarse particle Fresh catalyst, new H ₂ mass flow controller
C ₁	Exploratory	Standard, with coarse particle (re-used)
C ₂	Exploratory, halfway increase H ₂ flow	Standard, with coarse particle (re-used), after 90 min increase hydrogen flow to 50 mL/min

C ₃	Exploratory, lower liquid flow	Standard, liquid flow: 0.6 ml/min,
D ₃	High pressure, high gas flow (increased hydrogen concentration), unchanged residence time	Gas flow: 40 ml/min; pressure: 60 bar; liquid flow: 10 ml/min
E	No hydrogen (testing water evaporation in standard run)	Standard, but no gas flow
F ₁	Fine catalyst	Standard, fine catalyst
F ₂	Fine catalyst, lower temperature	Standard, Temperature: 80 °C
F ₂ '	Fine catalyst, lower temperature	Standard, Temperature: 70 °C
G	Low residence time (higher liquid and gas flows)	Standard, pressure: 60 bar; gas flow: 45 ml/min; liquid flow: 1.2 ml/min; Residence time approximately: 120 s

Table 3, exploratory experiments.

Experiments H_A-H_F and experiments I and I_B were done at different catalyst loadings. The catalyst loadings per experiment are shown in Table 4.

Experiment	Catalyst weight (g)	Filler weight (g)
H _A	1.64	0.21
H _B	1.39	0.49
H _C	1.21	0.74
H _{C2}	1.22	0.58
H _D	0.89	1.01
H _E	0.58	1.03
H _{E2}	0.61	1.20
H _F	0.41	1.38
H _{F2}	0.41	1.41
H _G	0.78	1.03
I	0.46	1.48
I _B	0.43	1.44

Table 4, catalyst loading for experiments H and I.

A series of additional experiments were done in the mini-scale packed-bed reactor. These experiments (labelled J_A–J_D) varied the amount of catalyst loading per experiment and within an experiment the gas flow and the reactor temperature were varied. An overview of the variations in flow and temperature is shown in Table 5. The time between samples is reduced to 15 min instead of 20 min. For this set of experiments the reactor is heated up and allowed time to reach a steady state before the experiment is started. When switching conditions the reactor is left at steady state for 15 minutes before continuing with the next sample. This is done to ensure that inside the reactor no traces of the previous reaction conditions are present.

Sample numbers	Gas flow (at normal conditions)	Reactor temperature (in °C)
----------------	---------------------------------	-----------------------------

1-3	40	90
4-6	50	90
7-9	30	90
10-12	30	80
13-15	30	100

Table 5, variations for experiments series J.

Table 6 shows the catalyst loading for the experiment series J. The catalyst loading is varied from 0.46 g up to 1.12 g. Filler material (SiC) is added to bring the total weight to approximately 1.8 g. For the experimental series H, I and J all the samples taken were analysed with H-NMR to determine the concentrations of LA, 4-HPA and GVL.

Experiment	Catalyst loading (in g)	Filler loading (in g)
J _A	0.46	1.56
J _B	0.60	1.21
J _C	1.12	0.72
J _D	0.53	1.32

Table 6, catalyst loading for experiment series J.

The concentrations in a sample was calculated using Equation 12.

$$C_{LA,out} = \frac{C_{LA,out}}{\text{Volume fraction sample in NMR}} \frac{\text{Intensity}_{LA}}{\text{Intensity}_{Dioxane}} \frac{8}{3}$$

Equation 12

The conversion of LA was calculated using Equation 13.

$$X_{LA} = \frac{C_{LA,in} - C_{LA,out}}{C_{LA,in}} \times 100\%$$

Equation 13

For the calculation of R_A Equation 14 is used.

$$R_A = (C_{LA,in} - C_{LA,out})\phi_V$$

Equation 14

3.4 Flow regime prediction

An accurate approximation of the flow regime in the mini-scale packed-bed reactor can be obtained from the Reynold number. In the literature many models have been given to predict the flow regime. Each model has a limited range for its validity. In this study it was found that the experimental setup for the mini-scale packed-bed can be predicted by a model by Ranade et al. and Fukushima et al. [16] [31]. In this model the Reynolds numbers for the gas phase and for the liquid phase are plotted against each other. Figure 9 gives an overview of the flow regimes based on the Reynolds numbers. To validate if the experiments in the mini-scale packed bed reactor fall within the trickle bed area the Reynolds numbers for both the gas and liquid phase are calculated for the typical reaction conditions as shown in

Table 2.

For the calculation of the Reynolds number Equation 15 and Equation 16 are used.

$$Re_{liq} = \rho_{liq} U_{liq} D / \mu_{liq} \quad \text{Equation 15}$$

$$Re_{gas} = \rho_{gas} U_{gas} D / \mu_{gas} \quad \text{Equation 16}$$

Where ρ_x is the density of the substance; U_x is the superficial velocity of the phase calculated by: volumetric flow rate/cross-sectional area of the reactor; D is the diameter of the tube and μ_x is the dynamic viscosity of the fluid. Values for the used parameters in Equation 15 and Equation 16 are given in Table 7.

Parameter	Value	Unit
ρ_L	1000	kg/m ³
U_L	2,12 * 10 ⁻⁴	m/s
D	0.01	m
μ_L	3*10 ⁻⁴	kg / (m*s)
ρ_G	1	kg/m ³
U_G	1,40 * 10 ⁻⁴	m/s
μ_G	1.02 * 10 ⁻⁵	kg / (m*s)
Re_L	5.5	
Re_G	5.0	

Table 7, values for parameters of Equation 15 and Equation 16.

This model gives the flow regime in the reactor if there is no packing of catalyst present, e.g. it gives the flow regime in the preheating section of the small reactor. Using the Reynolds numbers from Table 7 and inserting these values in Figure 9 the set of experiments for this study fall into the crosshatched area. It is clearly seen that trickle flow regime is dominating. It is clear that the values for the Reynolds number for both fluids are well below 2000. Therefore, laminar flow is expected.

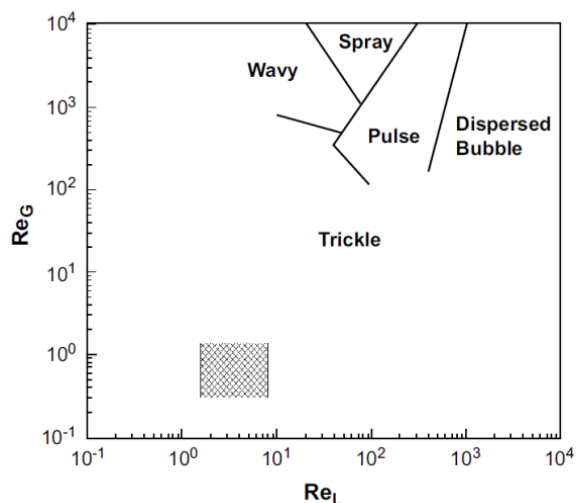


Figure 9, flow regime map [16] [31].

However in the packed bed, the parameters for Equation 15 and Equation 16 change. The characteristic length D becomes the particle diameter and an additional term is introduced for the porosity of the packing ε . This gives Equation 17 and 18. The value of voidage ε ranges between 0 and 1. The theoretical maximum packing density for spheres is 74 % [32]. The catalyst particles used in this study are assumed ellipsoid. The porosity is assumed to be around 0.7. This will give rise to an inaccuracy in the results, but this inaccuracy is believed to be small relative to the logarithmic scale of Figure 9. The average particle diameter is $4 \cdot 10^{-4}$ m.

$$Re_{liq} = \frac{\rho_{liq} U_{liq} D_{particle}}{\mu_{liq} \varepsilon} \quad \text{Equation 17}$$

$$Re_{gas} = \frac{\rho_{gas} U_{gas} D_{particle}}{\mu_{liq} \varepsilon} \quad \text{Equation 18}$$

For the packed bed used in the experiment under standard experiment conditions the Reynolds number calculated using Equation 17 and Equation 18 for the liquid phase and the gas phase are 7.0 and 0.2 respectively. When comparing these values with the flow regime map of Figure 9, the reactor is operated far away from the boundary conditions of the wavy, pulse or dispersed bubble flow. The prevailing flow regime can be safely assumed to be trickle flow.

3.5 Deriving a plot for mass transfer limitations

For the mass transfer limitations determination a plot is made between $C_{H_2(g)}/R_{H_2}$ (i.e., $C_A(g)/R_A$) versus $1/W$. In this plot $1/W$ is the independent variable and is the inverse of the catalyst weight added to the reactor volume. $C_{H_2(g)}/R_{H_2}$ is the concentration of hydrogen in the gas phase divided by the rate of reaction of hydrogen. Because LA and H_2 react stoichiometrically with each other the rate of reaction is

calculated by the amount of LA conversion per reaction time. The calculations are given in Appendix 8.2. For each data point in the plot multiple different samples as taken and the average values are used for the points in the plot.

Each data point is also reviewed if the data give a reliable result. For some samples the total concentration of active species is very low or high compared to the expected value of 1.2 mol/L. The cut off criteria for this selection are set to 0.8 mol/L as the minimum and 1.6 mol/L as maximum. Data points out of this range are discarded as not reliable.

3.6 Catalyst particle size analysis

The catalyst particle average size was derived by taken pictures of the particles with a ruler included in the frame. The image is then analysed using ImageJ software from the National Institutes of Health. Using the software the average particle size and standard deviation are calculated. This was done for the fresh coarse catalyst, fresh fine catalyst, fresh filler material and used fine catalyst-filler mixture. The pictures used can be found in Appendix 8.3. In ImageJ software, first the scale was set using the ruler in the picture. Then a selection in the picture was made where the particles lay evenly spread. Then the threshold was set to secure a good contrast between particles and background. Then the particles were analysed, the results were copied to an excel sheet where the diameter was calculated for each particle. The mean particle diameter and standard deviation of the mean were calculated.

3.7 Microreactor setup

The setup for the microreactor is similar to the setup for the mini-scale packed-bed reactor. A process flow diagram (PFD) for the microreactor is shown in Figure 11. The solution is fed to the reactor by a high pressure liquid pump (Hewlett Packard series 1100 BinPump G1312A) to achieve a liquid flow rate of 0.62 mL/min and maintain a pressure in the reactor of 45 bar. This liquid flow rate was chosen because it gives a steady flow and allows for a comparable gas-liquid flow ratio. Hydrogen gas from a cylinder is passed through a reducer to reduce the pressure to 45 bar, a mass flow controller is placed downstream from the reducer to regulate the mass flow of H₂ to the reactor. This is the same mass flow controller as used in the mini-scale packed-bed reactor setup. The mass flow of the gas phase is set to 19 mL/min. A one-way valve is inserted after the mass flow regulator to prevent back-flow of fluids. The gas and the LA solution are mixed using a T-junction where gas is inserted in the liquid flow. A schematic of the T-junction is shown in Figure 10.

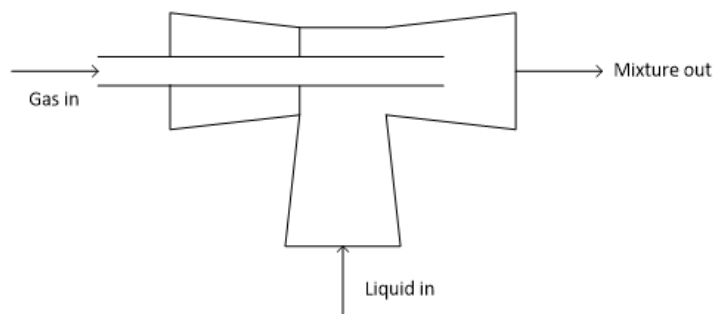


Figure 10, schematic of T-junction used for gas-liquid mixing.

Radel tube with an inner diameter of 1/16 inch (= 1.6 mm) and an outer diameter of 1/8 inch (= 3.2 mm) is used as the microreactor. The length of the packed bed is 0.3 m and a section of 0.3 m is added in front and after the packed bed to ease connecting the reactor on both sides and ensure that sufficient reactor

pathway can be placed in a heated water bed to guarantee the reaction mixture is at the set temperature before reaching the packed bed. The dry reactor is loaded with catalyst by using a Pasteur capillary pipette as a funnel. By tapping the tube and the funnel the catalyst can be loaded with relative ease. The volume of the packed bed is approximately 2.4 mL, which corresponds to a residence time of 140 s at given flow rates. The microreactor is placed in a custom made glass enclosure where heated water from a bath kept at 92 °C is pumped through in counter current flow. At the inlet and outlet of the glass enclosure the temperature of the water is measured using a thermometer. The catalyst bed is loaded with catalyst particle or a mixture of catalyst particles and silica carbide particles of similar particle size. The total mass of the packed bed is around 1.1 gram. For the mixture of particles the compounds are individually weighed in paper cups, then combined and shaken for approximately 20 s to ensure good macroscopic mixing. To remove used catalyst from the catalyst the packed bed was placed in an oven at 50 °C overnight to remove all water. The dry catalyst can then easily be removed from the tube.

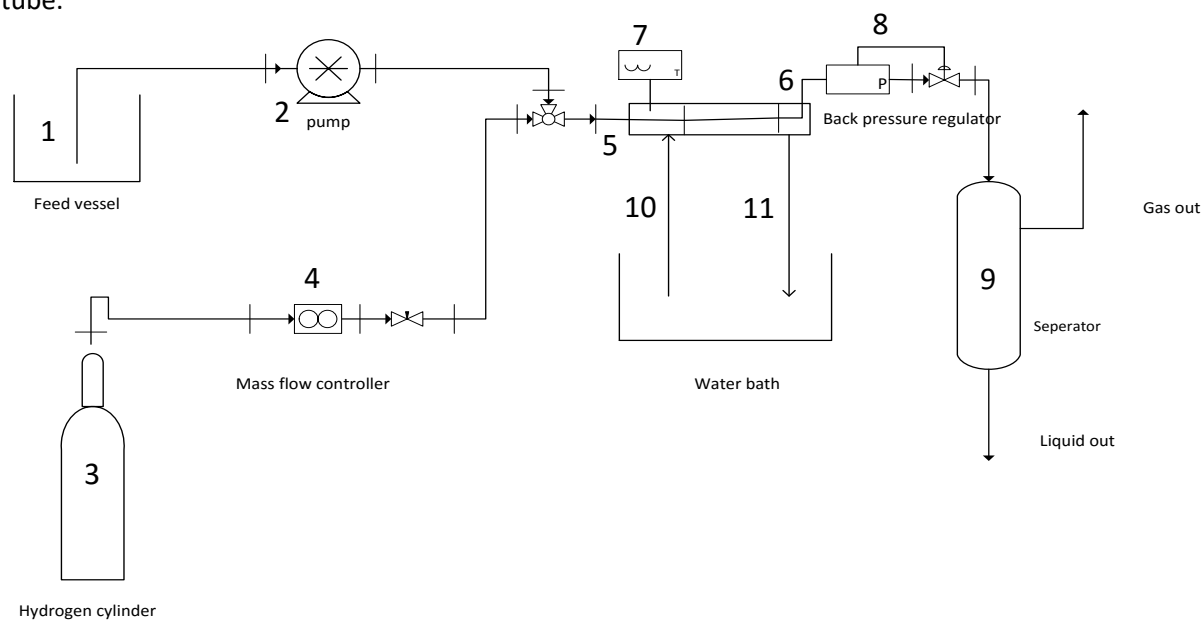


Figure 11, PFD for microreactor setup.

During setup it was found that operating the microreactor even without a packed-bed the gas and liquid flow rates have to be kept low. If either of the flow rates is increased above a threshold the flow pattern changes dramatically. And the slugs start overtaking each other and the slugs grow in size by conglomerating. The threshold values that were observed were 0.5 ml/min and 20 ml/min for liquid and gas respectively (gas rate at standard conditions).

In Figure 12 a photograph of the microreactor setup is shown. This is added to illustrate for future research how the setup can be used. The numbers in the photos are used to illustrate the different equipment used, the numbers are also shown in Figure 11.

The microreactor is placed inside the glass casing from the sides [5] and [6]. Inside the glass casing water of a specified temperature can be circulated using the inlet nozzles [10] and [11]. A HPLC pump [2] is used which draws the solution from a flask [1].

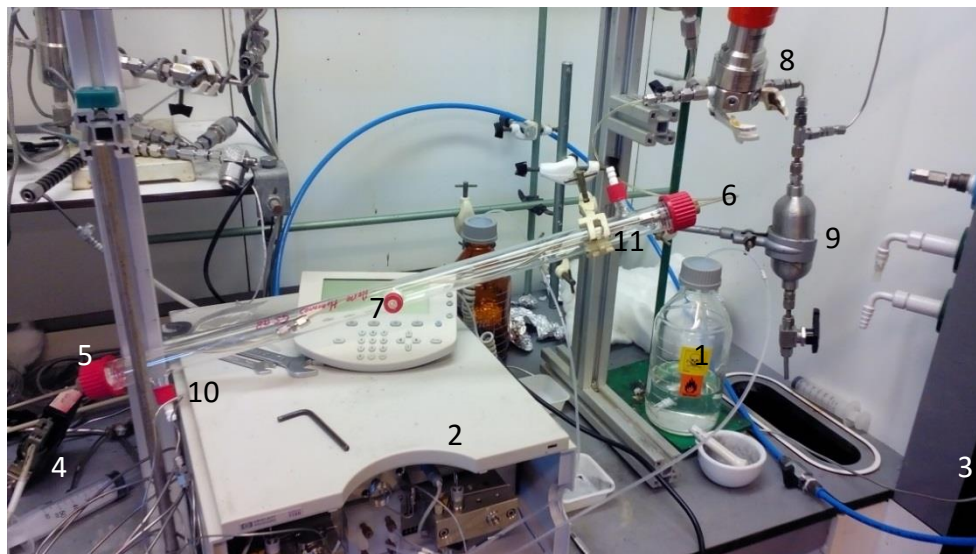


Figure 12, photograph of microreactor setup.

3.8 Flow pattern dependency on pressure in the microreactor

In the microreactor the flow pattern can be readily observed during operation. This allows for an analysis of the effect of pressure on the flow pattern in the tube. For this purpose the packed bed was initially removed from the tube. The setup was not heated and the fluids are assumed to be at room temperature. The gas flow was set at 20 ml/min and the liquid flow at 0.6 ml/min. At these conditions the inlet flow is approximately constant and the gas-liquid mixture shows regular slug flow even at low pressure ($p = 5$ bar). The slug flow is disrupted by the mesh present in the connector. The mesh is placed there to prevent catalyst particles from being carried out of the bed by the fluids. The result of this disruption is that the slugs of gas and liquid combine and grow.

The gas-flow ratio is kept steady and the back-pressure regulator is used to increase the pressure in steps of approximately 5 bar up to 40 bar. The change of flow in the tube is documented by photographing the plug flow at the inlet and the outlet of the tube. The average length of a slug is determined by measuring the sum of the length of a fluid and dividing the sum by the amount of slugs in the frame. This is done to determine under what conditions stable slug flow can be steadily achieved and during future microreactor testing to be able to compare the flow patterns in the packed bed to flow without obstruction.

4 Results & Discussion

4.1 Experiments

After the first 2 experiments in the mini scale reactor the conversion using coarse catalyst was consistently around 80%. Increasing the hydrogen concentration by 33% resulted in increasing the conversion to 90%. Using finer catalyst also was useful to increase the conversion, in experiment F1 the average conversion reached 99%. This could be an indication that the reaction already achieved completion before the end of the packed bed. In experiment F2 and F2' the temperature was lowered to 80 and 70 °C respectively, the conversion reached was 93% and 96% respectively. It is expected that

lowering the temperature would lower the conversion, this is not clearly observed from the experiments. In Experiment G the effect of reducing residence time was not observed to have a strong effect on the conversion. For Table 8 and Table 9 the final column shows the maximum difference with the mean, to serve as an indication for the reproducibility of the results. A low deviation shows a high consistency of results within that experiment.

Experiment	Goal	Conditions	Average conversion (% of LA reacted)	Maximum deviation from mean conversion (%)
A	Exploratory	Standard, with coarse particle	25	13
B	Exploratory	Standard, with coarse particle Fresh catalyst, new H ₂ mass flow controller	64	1
C2	Exploratory, halfway increase H ₂ flow	Standard, with coarse particle (re-used), after 90 min increase hydrogen flow to 50 mL/min	78	3
C3	Exploratory, lower liquid flow	Standard, liquid flow: 0.6 ml/min,	83	5
D3	High pressure, high gas flow (increased hydrogen concentration)	Gas flow: 40 ml/min; pressure: 60 bar; liquid flow: 10 ml/min	90	9
E	No hydrogen (testing water evaporation in standard run)	Standard, but no gas flow	0	0
F1	Fine catalyst	Standard, fine catalyst	99	2
F2	Fine catalyst, lower temperature	Standard, Temperature: 80 °C	93	10
F2'	Fine catalyst, lower temperature	Standard, Temperature: 70 °C	96	2
G	Low residence time (higher liquid and gas flows)	Standard, pressure: 60 bar; gas flow: 45 ml/min; liquid flow: 1.2 ml/min	98	2

Table 8, exploratory experimental results.

In Table 9 an overview of the results from the set of experiments with the variations in catalyst loading is shown.

Experiment	Catalyst weight (g)	Filler weight (g)	Mean conversion (%)	Standard deviation (%)
H _A	1.64	0.21	96.5	5.7
H _B	1.39	0.49	96.2	1.1
H _{C3}	1.21	0.74	62.5	3.2

H _{C2}	1.22	0.58	94.0	2.6
H _D	0.89	1.01	46.6	2.9
H _{E3}	0.58	1.03	19.0	3.1
H _{E2}	0.61	1.20	76.3	3.8
H _{F3}	0.41	1.38	12.7	0.2
H _{F2}	0.41	1.41	38.3	3.2
H _G	0.78	1.03	75.6	3.9
I _A	0.46	1.48	28.2	3.0
I _B	0.43	1.44	28.3	5.8

Table 9, experiments set for mass transfer limitations identification.

4.1.1 Conversion vs. catalyst loading

Initial results of conversion for different catalyst weight are shown in Figure 13. With increased catalyst added the conversion approaches 100%. The error bars in Figure 13 show the standard deviation of the deviation in the measurements. The deviation can be considered a measure of the accuracy of the NMR analysis and the constant reaction conditions. Assuming during a single experiment the conditions are kept constant, the error bars give an indication of the inaccuracy of the NMR results. The highest value for the standard deviation is 6.7 %, and the mean standard deviation is 3 %. NMR spectroscopy is an incredibly useful tool for identification of chemical species. However, for calculation of the inverse of the reaction rate ($1/R_{H_2}$) NMR spectroscopy is less accurate. Because of the high variations in the mass balance per experiment and through further calculations the error can be multiplied.

Increasing the catalyst weight in the reactor will reduce the reaction resistance according to Equation 8. The kinetic resistance should reduce by the square of the catalyst weight increase. The liquid-solid resistance should reduce linearly. Figure 13 does not show a clear quadratic correlation but rather a linear correlation. This is an indication that the kinetic resistance is not rate limiting.

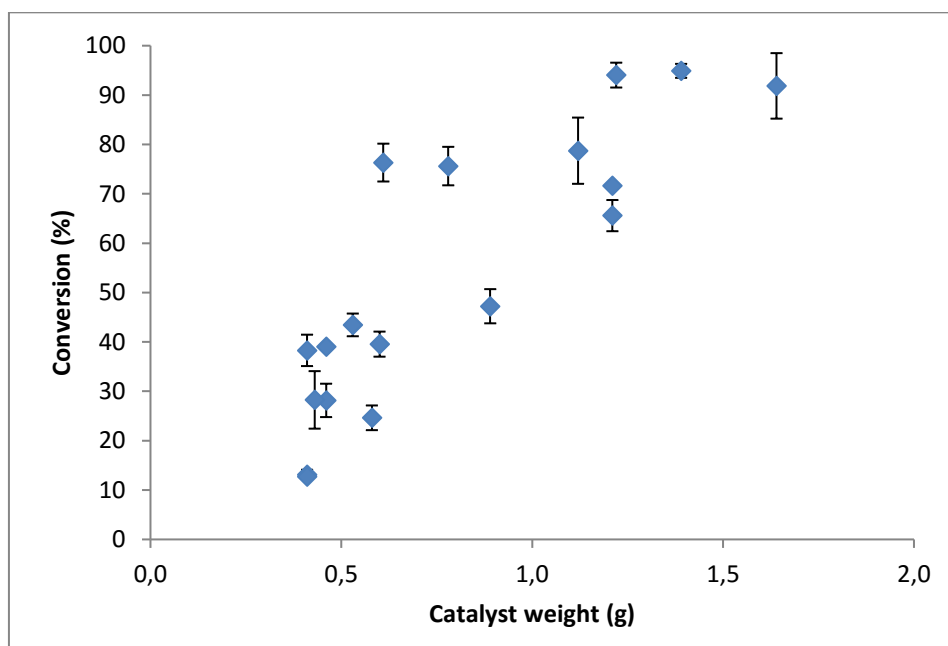


Figure 13, plot of conversion vs. catalyst weight.

4.1.2 Reproducibility of experiments

The reproducibility of experiments has been examined by performing certain experiments in duplo or triplo. The reproducibility can be seen in Figure 13 where it is clear that the conversion for the same catalyst loading can vary up to 30 %, which is very high. This inaccuracy reduces the conclusions that can be drawn in this study.

4.1.3 Variations in flow ratio

In Figure 14 the results for the experiments with varying gas-liquid ratios is shown. The liquid flow rate, pressure and temperature are kept constant and the gas flow is varied from 30 - 50 ml/min. The error bars show the standard deviation per flow rate.

The diamond shaped points show the values corresponding to the standard conditions (30 ml/min). The square shaped points correspond to a small increase in gas flow rate, and as such are expected to have a higher rate and therefore show lower values for $1/R_{H_2}$. The circular points correspond to an even higher gas flow rate, and are expected lowest in the chart. The data points for the 40 data series are consistently lower than the data points for the 40 ml/min data series. For the lowest catalyst weight the data lies farther apart and the results show less reliability. The data points for the higher catalyst loading lie quite close to each other. This shows that changing the gas-liquid flow ratio does not significantly affect the reaction rate at lower catalyst weight. This implies that gas-liquid transfer is not rate determining at lower catalyst weight.

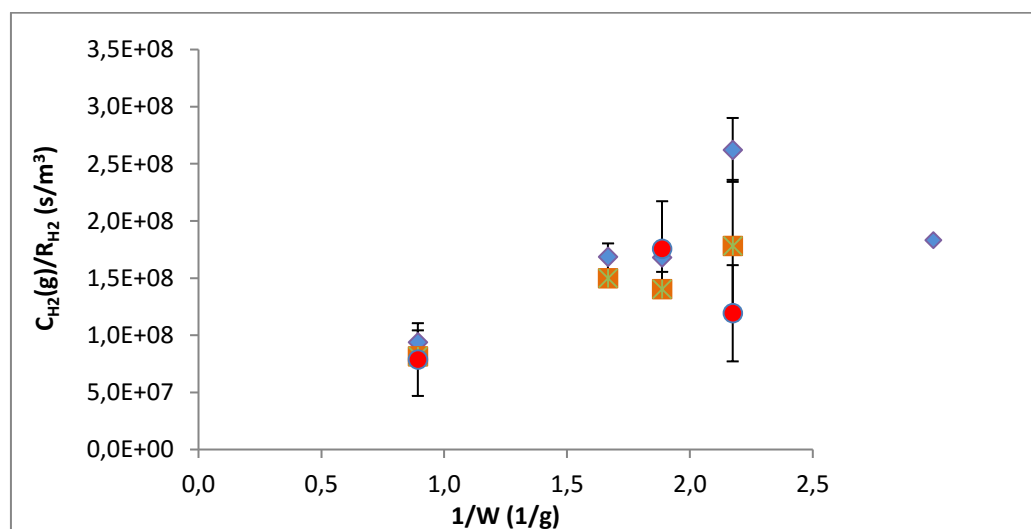


Figure 14, plot of $C_{H_2(g)}/R_{H_2}$ vs $1/W$ for different gas flows.

4.2 Kinetic model analysis

To study the effects of varying variables and compare the kinetically limited and mass transfer limited rate a model was made using Excel software. The model is based on Equation 8 which is repeated here for reader convenience in Equation 19.

$$\frac{C_{H_2(g)}}{R_{H_2}} = \frac{H}{V k_l a_i} + \frac{H}{W} \frac{1}{k_c a_c} + \frac{H R_{H_2}}{(W \eta k)^2}$$

Equation 19

The parameters in Equation 19 can be found using the correlations as shown in Table 10.

Parameter	Correlation	Value	Unit	Source
Gas-liquid mass transfer coefficient	$k_l a_i = 8.08 \left(\frac{G_L}{\mu_L} \right)^{0.41} S_c^{1/2}$	$2.69 * 10^{-3}$	s^{-1}	[30]
Schmidt number	$S_c = \frac{\mu_L}{\rho_L D}$	$5.45 * 10^{-3}$		[30]
Sherwood number	$Sh = 0.815 Re_l^{0.822} S_c^{1/3}$	$3.33 * 10^{-1}$		[30]
Bulk liquid-to-solid interface (Re < 20)	$k_c = \frac{Sh D}{d_p}$	$3.05 * 10^{-2}$	m/s	[30]
Effectiveness factor	η	range 0 – 1		
Kinetic constant	$k = A \exp\left(-\frac{E_A}{R T}\right)$	$6.3 * 10^{-3}$	mol/(g*s)	[11]

Table 10, correlations used in Equation 19.

4.2.1 Gas-liquid resistance

In Equation 19, $\frac{H}{V k_l a_i}$ represents the contribution of the gas-to-liquid absorption to the overall resistance. H is constant for a given temperature and pressure; V is the reactor volume and $k_l a_i$ is the mass transfer coefficient gas-liquid.

4.2.2 Liquid-solid resistance

$\frac{H}{W k_c a_c}$ is the contribution of the liquid-to-solid diffusion of hydrogen to the overall resistance. W is the catalyst weight; k_c is the bulk liquid-to-solid interface which is dependent on T and particle size and a_c is the specific surface area of the catalyst which is a function of the particle size.

4.2.3 Kinetic resistance

$\frac{H R_{H_2}}{(W \eta k)^2}$ is the kinetic resistance combined with the resistance of intra-particle diffusion of hydrogen within the catalyst pores to the overall resistance to the reaction. R_{H_2} is the overall reaction rate (in mol/s), η is the effectiveness factor for the catalyst, a measure of how much of the catalyst surface is accessible to the reactants. k is the intrinsic reaction rate is determined using the Arrhenius equation.

The concentration of gas in the gas remains constant because only pure hydrogen is present in the gas phase and the pressure remains constant. The reactor volume (V) is constant for all experiments. The Henry constant (H) and the coefficients (k_l , k_c and k) are constant as long as the temperature is kept constant. The gas-liquid interfacial area will change as hydrogen reacts with levulinic acid. If all of the LA has reacted only 16.6 % of the gas will be left. Because the pressure in the reactor is constant, this means the volume of the gas will decrease. The total volume of water will remain the same, so the total interfacial area will decrease. An assumption is made here that the concentration of LA and H_2 is

constant and independent from the position in the reactor. This is justified for experiments where the conversion is low as the difference between the inlet and outlet concentration doesn't change considerably.

In the model it is possible to consider cases where the rate is determined by either (i) mass transfer resistance from gas to liquid, or (ii) the mass transfer resistance from liquid to solid, or (iii) reaction kinetics.

Figure 15 shows the result for this comparison. In this chart the blue horizontal line corresponds to the gas-liquid resistance, the purple line corresponds to the liquid-solid resistance, the green line corresponds to the kinetic resistance. The red line is the sum of all the resistances and is equal to $\frac{C_{H_2(g)}}{R_{H_2}}$. From Figure 15 it is not clearly seen that the slope of the green line (kinetic resistance) is not 0 because it is significantly smaller than the other contributions.

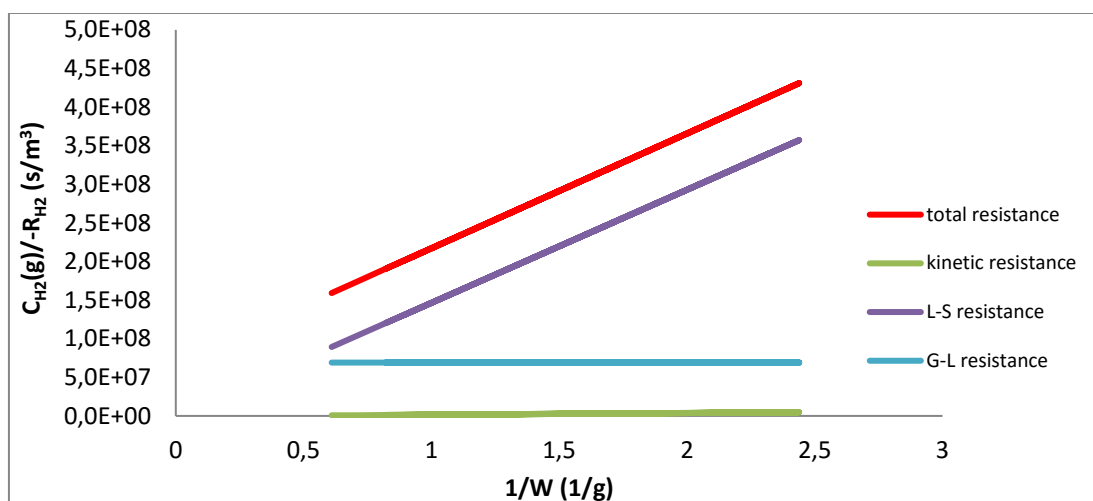


Figure 15, model resistances.

4.2.4 Mass transfer limitations

4.2.4.1 Standard conditions

In Figure 16 the experimental results are shown in the same graph as the model results. Even though the experimental data varies from experiment to experiment the trend in the numerical model does fit the experimental trend. To improve the fit of the model with the experimental data the parameters of the model are assessed individually in the next paragraph.

In the graph horizontal-axis shows the inverse of the weight, the vertical axis shows a constant ($C_{H_2(g)}$) divided by reaction rate. The error bars (based on the standard deviation of the average of each experiment) for the data points are shown to identify the accuracy of each data point. In this model η is initially assumed to be 1, in paragraph 4.2.6 this assumption is evaluated.

This shows that the reaction resistances can be visualised. The model parameters are evaluated to allow a closer fit between the experimental and numerical data. From this plot it is concluded that the contributions of mass transfer are dominating the rate limitations. At high catalyst weight the resistance contributions of diffusion and absorption are about equal. When the amount of catalyst is lowered the contribution of liquid-to-solid diffusion becomes dominant. By using microreactors the mass transfer resistances can be lowered in 2 ways. First, by lowering the gas-to-liquid resistance by increasing the gas-

liquid interface area which will increase $k_l a_l$. Second, by lowering the liquid-to-solid resistance by using smaller catalyst particles, which will increase $k_c a_c$.

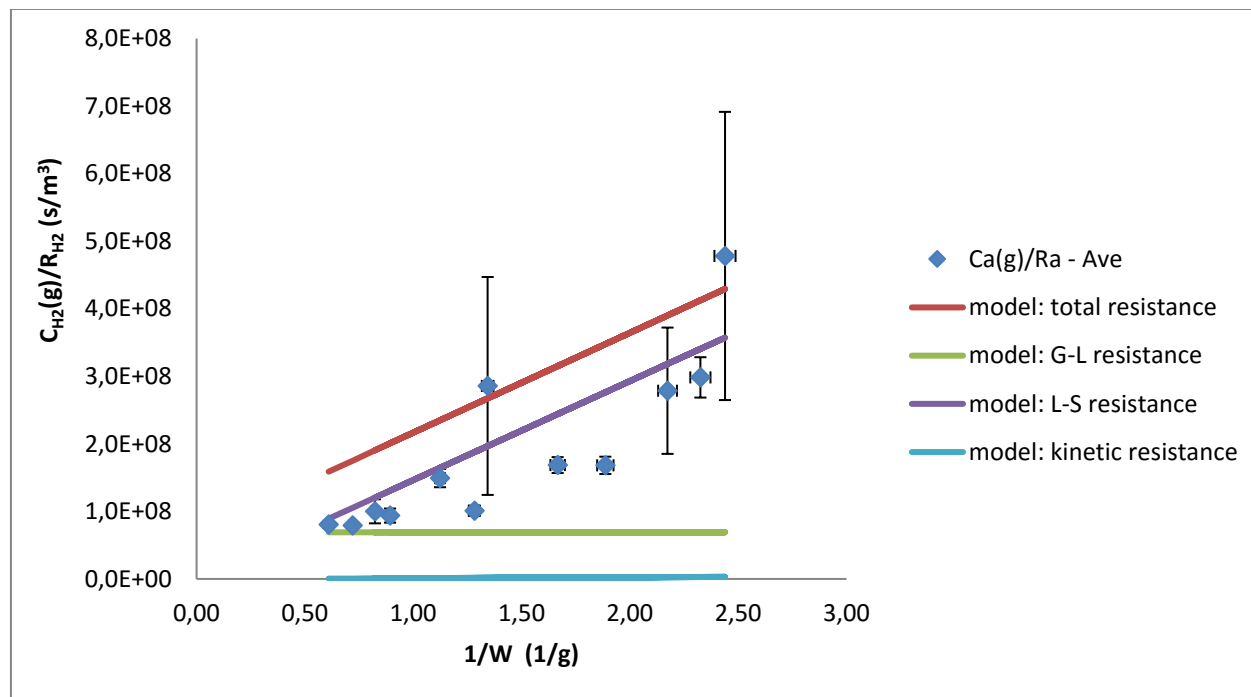


Figure 16, kinetic model compared with experimental results.

4.2.5 Model Temperature dependency

A set of experiments was designed to investigate the effect of temperature on $C_{H_2(g)}/R_{H_2}$ the results of these experiments are shown in Figure 17. The diamond shaped points show the values corresponding to the standard conditions. The triangle shaped points correspond to lower temperature conditions, and as such are expected to have a lower rate and therefore show higher values in the plot. The cross shaped points correspond to the reaction at 100 °C, these points are expected to have the highest rate and therefore the lowest in the chart. This trend is not clearly observed.

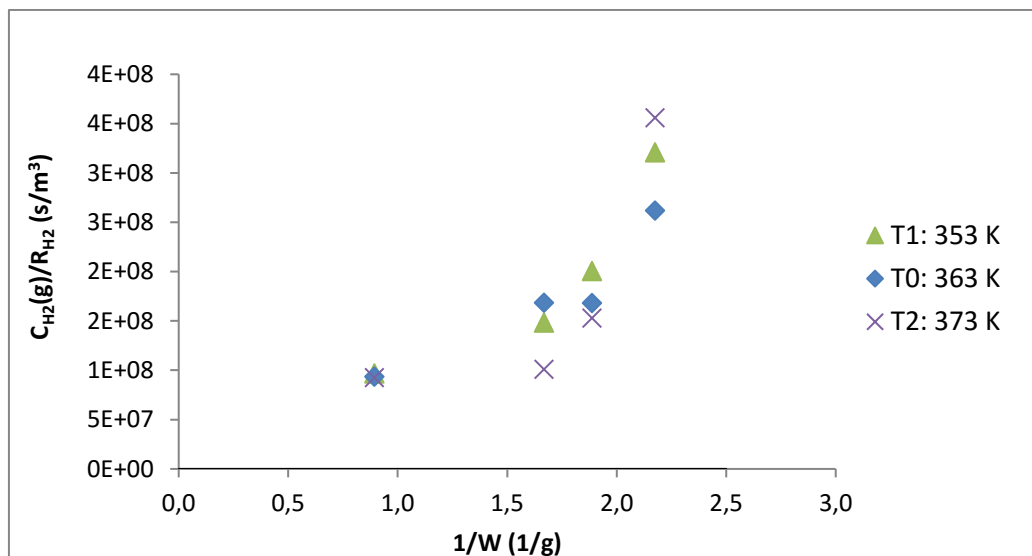


Figure 17, effect of temperature variations (experimental).

Using the model a plot was made of the effect of temperature on $C_{H_2(g)}/R_{H_2}$ was plotted for $1/W = 0.6$ $1/g$, this plot is shown in Figure 18. Although temperature does not directly appear in Equation 19, it does influence a number of parameters. The affected parameters are the kinetic constants (k_i , k_c and k), the gas concentration ($C_{H_2(g)}$) and the Henry constant H . From the graph it is apparent that for lower temperature the reaction becomes kinetically dominated. The kinetic resistance becomes small for higher temperatures. In our experiments, the temperature was varied from 353 – 373 K. Comparing with the model reveals that at these conditions changing the temperature by 10 K will have a limited effect on the overall resistance. An increase of the temperature from 353 to 363 K will decrease $C_{H_2(g)}/R_{H_2}$ by 4.0 %, a further increase in the temperature from 363 to 373 K will decrease $C_{H_2(g)}/R_{H_2}$ by 3.4 %. In the experimental data the trend of higher temperature leads to higher reaction rate is not clearly observed. From paragraph 4.2.4.1 it was learned that the average error per experiment was 3 %. Considering this possible error in the experimental results in Figure 17 it can be concluded that the experimental data does follow the predicted trend.

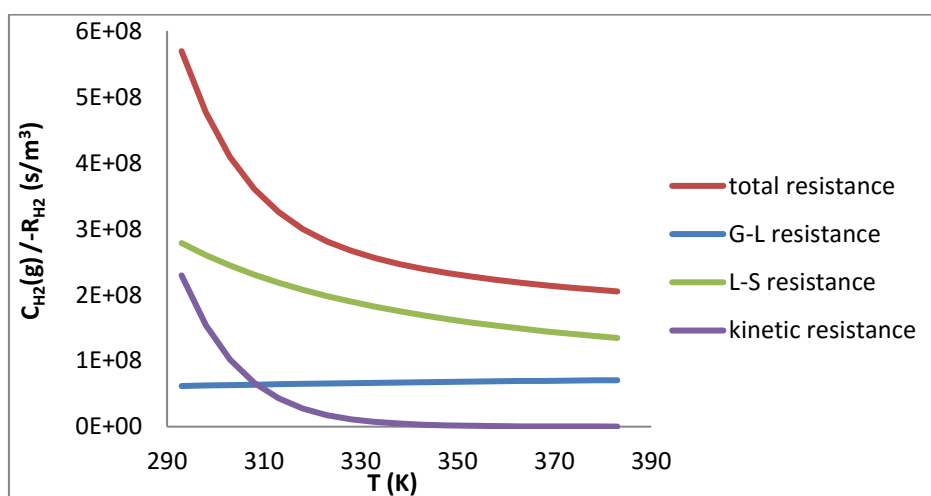


Figure 18, model results for varying temperatures.

4.2.6 Model effectiveness factor dependency

For porous catalyst some active sites are not very easily accessible due to narrow pores, constrictions in the pores or bends. This means that within some pores the concentration of reactants is lower than on the catalyst external surface. The effectiveness factor (η) is a measure of how much of the catalyst active sites are accessible to the reactants. Figure 19 shows the resistances as a function of the effectiveness factor. From this plot it is seen that for values of $\eta > 0.2$ the contribution of the kinetic limitations is small relative to the mass transfer limitations. For values of $\eta < 0.2$ the kinetics increase rapidly and for $\eta < 0.1$ the kinetics become dominating for the rate limitations. Previous research suggests typical values for these catalysts and conditions to be in the range of 0.7 – 0.95 [13]. From Figure 19 it is clear that the effect of the effectiveness factor doesn't play a significant role in the overall reaction rate.

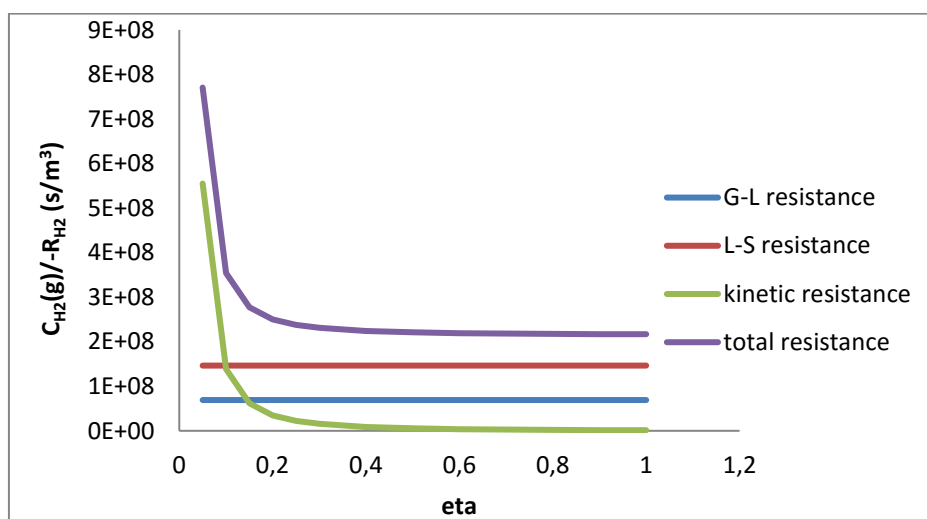


Figure 19, effect of effectiveness factor on overall rate resistance.

4.2.7 Model coarse vs. fine catalyst

In the first set of experiments it was observed that the catalyst particle size had a strong effect on the conversion. The larger particles yielded a lower conversion compared to the fine catalyst particles under the same reaction conditions. Using the model this effect was investigated by plotting $C_{H_2}(g)/R_{H_2}$ for $1/W = 0.6$ 1/g against the specific area (a_c) of the catalyst, as shown in Figure 20. The fine catalyst (mean $d_p = 0.8E-4$ m) has an $a_c = 5 E-3$ m²/g, while the coarse catalyst (mean $d_p = 1.2 E-4$ m) has an $a_c = 3 E-3$ m²/g. From this plot is apparent that the catalyst particle size has clear effect on the mass transfer through the liquid phase. It is also clear that changing from the coarse catalyst to the fine catalyst has a large effect on the conversion by increasing the diffusion resistance. In Figure 20 typical experimental data points for coarse and fine catalyst particles are drawn to show the correlation of the model to the experimental results. The datalabels displayed in Figure 20 give the values of $C_{H_2}(g)/R_{H_2}$ for the catalyst particle sizes. As in paragraph 4.2.4.1 the model gives a higher value for the overall resistance than the experimental data. The slope between the two experimental data points has a lower value than the slope of the line of the total resistance, but the slopes are of the same order of magnitude.

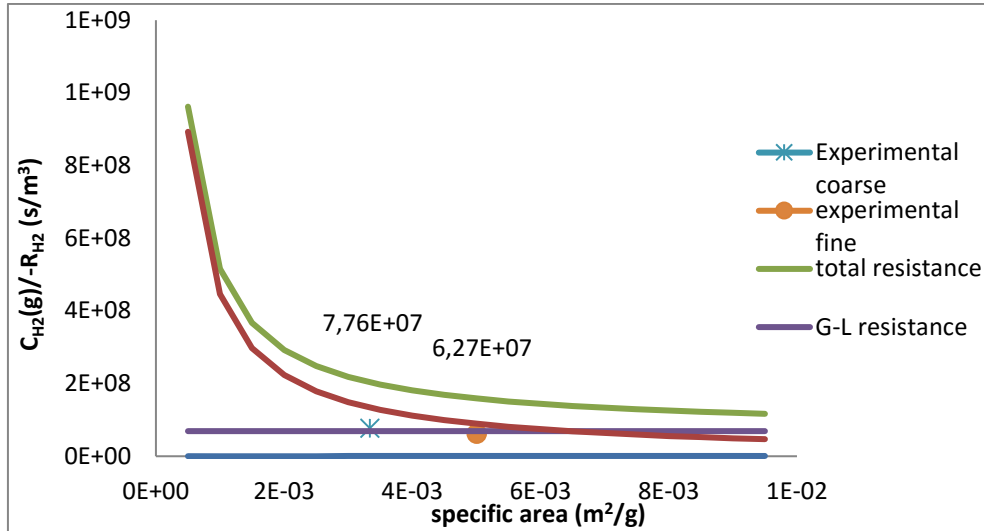


Figure 20, $C_{H_2(g)}/R_{H_2}$ vs. specific area for a fixed catalyst weight.

4.2.8 Estimation of $k_l a_i$

For Equation 8 an estimation for the value of $k_l a_i$ is used. In literature a number of correlations exist for $k_l a_i$ [27] [30] [31] [33] [34]. Table 11 shows 3 correlations that are used for trickle packed bed reactors with a concurrent gas-liquid flow.

Source	$k_l a_i$ (1/s)	Correlation used	Reference
Fogler	$5.95 \cdot 10^{-2}$	$\frac{k_l a_i}{D} = 8.08 \left(\frac{G_L}{\mu_L}\right)^{0.41} \left(\frac{\mu_L}{Sh * D \rho_L}\right)^{0.5}$	[30]
Iliuta et al.	$6.40 \cdot 10^{-1}$	$2.13 \cdot 10^{-3} \leq k_l a_i \leq 7.04$	[33]
Fukushima et al.	$3.43 \cdot 10^{-2}$	$\frac{k_l a_i d_p^2}{D \left(1 - \frac{\varepsilon_L}{\varepsilon_B}\right)} = 2 \left(\frac{a_c}{d_p^2}\right)^{0.2} Re_L^{0.73} Re_g^{0.2} \left(\frac{\mu_L}{D \rho_L}\right)^{0.5} \left(\frac{d_p}{D}\right)^{0.2}$ For: $\frac{dp}{D} \approx 0.01-0.07, \left(1 - \frac{\varepsilon_L}{\varepsilon_B}\right) \approx 1$	[31] [34]
Initial estimate	$3.00 \cdot 10^{-1}$		

Table 11, correlations used for $k_l a_i$.

Figure 21 shows a plot of $C_{H_2(g)}/R_{H_2}$ against $k_l a_i$. It becomes clear that the gas-liquid resistance becomes too large to fit with the experimental results for $k_l a_i < 0.3$. This means that the correlations from the second study can be valid. The other correlations found cannot be used for this study. These correlations have a scope for validity in terms of reactor diameter and volume as well as liquid and gas flow rates, temperature and pressure conditions.

The experimental conditions in this study are deemed to fall outside the scope of the validity of the studies by Fukushima et al. and the book by Fogler [30] [34].

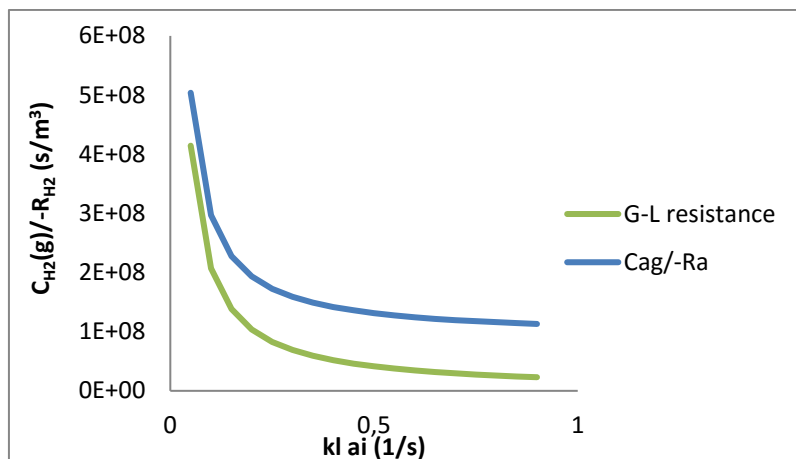


Figure 21, effect of $k_1 a_i$ on $C_{H_2(g)}/R_{H_2}$.

4.3 Microreactor

4.3.1 Setup testing

During cold-flow experiments in the microreactor gas leakage and back flow of liquid in the gas stream caused substantial flow pattern disturbances. The leakages were visualised by spraying a soapy solution on each connection and observe if bubbles were formed by escaping gas. The liquid back flow and flow pattern disturbances ceased after the leaks were fixed and the gas pressure was allowed to build up in the gas stream.



Figure 22, burst microreactor tube.

After cold flow testing yielded steady controllable slug flow a packed bed section was inserted. Initially slug flow was observed but gradually the flow became stagnant and the pressure in the packed bed was rising. The pressure at the back pressure regulator remained at ambient pressure. This resulted in bursting the micro tube at the connector as shown in Figure 22. The pressure build-up was caused by a blockage in the connector at the back end of the packed bed. The blockage was caused by the use of filter paper in the connector. The filter (seemed too small in mesh size) was added to prevent fine catalyst powder to be entrained by the fluids and causing harm to the back pressure regulator. Subsequently the filter paper was replaced by metal filter with a higher mesh size and the catalyst

particles loaded in the microreactor were filter screened to remove all the fine powder. Due to time constraints no further testing with the microreactor was done.

4.3.2 Flow pattern dependency on pressure

In a microreactor a cold flow test was done to compare the gas-liquid volumetric flow ratio for different pressures. For all pressures fairly regular slug flow is observed. However at higher flow rates the system is observed to undergo pulse flow. In the pulse flow the gas slugs can overtake the liquid slugs, this leads to slug agglomeration. This behaviour is deemed to be undesirable. In Table 12 the length of the bubbles is shown. In the last column the ratio of the average gas to liquid is calculated. At low pressure the gas bubbles are clearly larger in volume than the liquid bubbles. At higher pressures this trend is reversed, this is expected as at elevated pressure the gas is compressed while the liquid is incompressible.

Pressure (bar)	Picture	Average gas bubble length (mm)	Average liquid bubble length (mm)	Gas-liquid volume ratio
8	Figure 25	3.5	1.1	3.2
	Figure 26	4.6	1.3	3.5
12	Figure 27	3.5	1.3	2.7
	Figure 28	3.9	0.9	4.3
20	Figure 29	2.1	2.4	0.9
	Figure 30	2.1	1.9	1.1
	Figure 31	2.5	1.4	1.8
25	Figure 32	1.3	4.0	0.3
	Figure 33	1.1	2.4	0.5
35	Figure 34	1.6	3.8	0.4
	Figure 35	1.9	4.5	0.4
40	Figure 36	2.1	2.8	0.8
	Figure 37	2.3	3.7	0.6
	Figure 38	2.3	2.9	0.8
45	Figure 39	1.8	3.8	0.5
	Figure 40, used fine catalyst and filler (1).Figure 40	2	3	0.7

Table 12, flow pattern analysis.

The data from Table 12 can be used to derive a plot for the volumetric ratio of gas-liquid at different pressures, as shown in Figure 23. In the plot the theoretical gas-liquid ratio (based on the ideal gas law) is added. This shows that the experimental data corresponds well with the numerical values. This validates using the ideal gas law to relate the gas-liquid volume ratio to the pressure in future experiments.

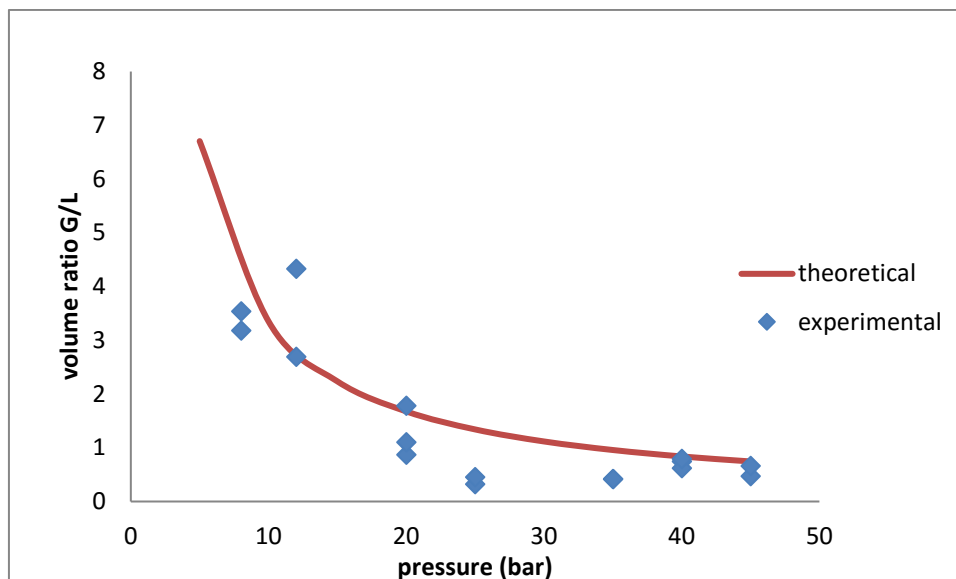


Figure 23, gas-liquid volume ratio at varying pressures.

4.4 Particle size distribution

In Table 13 the results for the particle size distribution analysis are shown. In a few cases several particles were grouped into a single measurement. To prevent a distorted representation of the particle size and distribution the values for particles over 2 mm were discarded. This is justified by examining the pictures where none of the particles exceed 2 mm in diameter. The average particle size for the used catalyst and filler mixture seems to be consistent between the pictures. For the coarse particles the standard deviation is higher and the mean diameter is more inconsistent between the two images. For the fine catalyst the results of the two measurements also differ a bit from each other. The results for the filler are consistent with each other.

Mixture	Picture	Mean particle diameter (mm)	Standard deviation (mm)
Used cat + filler	Figure 40	0.43	0.20
	Figure 41	0.37	0.18
Coarse catalyst	Figure 42	1.30	0.61
	Figure 43	1.06	0.79
Fine catalyst	Figure 44	0.94	0.26
	Figure 45	0.63	0.60
Filler (SiC)	Figure 46	0.42	0.24
	Figure 47	0.39	0.30

Table 13, particle size as derived using ImageJ software.

4.5 Reproducibility

Throughout the experiments it was seen that the reproducibility of the results was low. With conversion for a certain set of conditions ranging up to 30 %. This proved problematic for this study. Some possible explanations for this are given in this paragraph.

4.5.1 Catalyst mixing

At lower catalyst loading the reproducibility of experiments is more difficult than expected. One possible explanation for this behaviour could be that the catalyst and filler mixture are not uniformly mixed. Although attention is given to mix the powder carefully, it is possible that uniform distribution of powders is not achieved due to the difference in particle size and weight. When a vessel containing a mixture of powders is agitated it is common for segregation to occur. A consequence of segregation in a packed bed could be the formation of channels in the bed. Another possibility is that there are pathways formed for the reaction mixture where the reactants bypass sections of catalysts and only pass through the filler particle sections. This could have a significant effect on the conversion of the reactants [35].

4.5.2 NMR analysis considerations

It was found that a number of samples had a great variation in the mole balance. Possible reasons for these data points not being reliable could lie in the preparation of the NMR samples. It is found that for some samples the mixture in the tube was not well mixed and a part of the solution could be stuck to the top of the tube in tiny droplets. Small fluctuations in this steps result in large deviations in the calculated conversion, and even larger offsets in the calculated rate of reaction. For this reason the data points corresponding to samples where the mole balance doesn't fit are not used. The expected sum of the concentration of all components (LA, GVL and 4-HPA) is 1.2 mol/L. If the sum of the concentrations is lower than 0.8 mol/L or higher than 1.6 mol/L are not used in the data analysis. For this reason samples that gave a high deviation in the measured concentration were excluded from the data set. When discarding these samples the average error measured using NMR was 3 %.

4.5.3 Residence time variations

Another variable to be considered is the residence time of the reactants. It was observed that the flow rate of the liquid was not constant. Some samples taken had more liquid than others after an equal amount of time had passed. This could be caused by fluctuations in the air pressure powering the liquid pump. Because the air supply to the pump was also used simultaneously by other researchers, the air flow to the pump can fluctuate.

In the packed bed it is possible that the flow patterns cause a build-up of certain reactants. Which results in some reactants to be retained in a 'dead-zone' in the reactor whilst other reactants move quicker than average through the reactor. This can also cause variations in the conversion and therefore also in the calculated reaction rate. In another study the hydrogenation rate was observed to be independent of the bed dilution, which suggests that no dead-zones or residence time variations occur [11].

4.6 Catalyst deactivation

In this study for each new experiment fresh catalyst was used. Some experiments last longer, e.g. experiments J_{A-D}), for these cases catalyst deactivation needs to be considered. Catalyst deactivation can be caused by leaching of the active species or because of metal sintering. Both mechanisms of deactivation have been investigated in a previous study [5]. In this study the leaching was examined and it was found that although initially some leaching occurred this quickly became zero. The effect of sintering was also observed but only to a limited extend. The loss of kinetic activity over a 100 h period was found to be around 0.2 %/hour. The longest time on stream that the catalyst was in this study was 8 hours. Considering the deactivation rate this would cause a 1.6% reduction in activity. This reduction is smaller than the expected error from the analysis method. Also in the data analysis no evidence for

significant catalyst deactivation was observed. Therefore catalyst deactivation is not deemed to be a significant factor.

However if the study is translated to industrial scale using a microreactor this effect can become more problematic. Especially since microreactors are not as conveniently loaded with fresh catalyst as larger reactors because of more likely blocking in the narrow tubes.

4.7 Catalyst recycling

Catalyst recycling has been considered for this study. As ruthenium is a valuable metal recycling the catalyst would be preferable. In the literature many patents exist for ruthenium recycling, this shows that there is also a strong incentive from the industry to find an economic method for catalyst recycling. However the academic papers on the matter were not found.

4.8 Catalyst particle size distribution

The calculated diameter for the particles assumes that all particles are spherical. When the particles are inspected closer it is clear that this is not the case. This assumption was useful for giving an indication of the particle size distribution. Also it should be noted that the particles are generally longer along one axis than along others. This leads to a behaviour where the majority of the particles will favour laying with an elongated side down on the surface on which the particles are photographed. This leads to the particles appearing larger than they are in reality.

4.9 Scale up

As discussed in literature scaling up a process using a packed bed requires some careful consideration [10]. The pressure drop in the lab scale packed-bed reactor is negligible, but the pressure drop is a strong function of the bed length and volumetric flow rate. This could potentially become problematic for large setups.

5 Conclusion

In the search for alternatives for fossil fuels chemicals, biobased platform chemicals can play an integral role. One important bio-based platform chemical is γ -valerolactone that can be used as a feed for solvents, bulk chemicals and intermediates for fine chemicals. In literature the focus of the study of the hydrogenation of LA to GVL generally lies on the intrinsic kinetics rather than the mass transfer limitations. In the mass transfer limited regime the catalyst is not used as efficient as possible. For industrial application of LA hydrogenation to GVL making efficient use of expensive catalyst increases the feasibility of the process.

The objective of this study was to identify and compare the contributions to the rate limitations for the hydrogenation of LA to GVL over Ru/C catalyst particles. The mass transfer of hydrogen to the catalyst external surface was hypothesised to be rate limiting under the reaction conditions of this study. A series of experiments was carried out in a continuous mini-scale packed-bed reactor with varying catalyst loading.

The experimental results were compared to a numerical model for the reaction rate. The combination of hydrogen absorption to the liquid and diffusion of hydrogen to the catalyst external surface was found

rate determining rather than the kinetics on the catalyst surface. For lower catalyst weight, the limitation with hydrogen diffusion through the liquid to the catalyst external surface tends to be more dominating.

For particle size the difference in conversion between coarse particles ($1.25 \text{ mm} < D_p < 2.5 \text{ mm}$) and fine particles ($0.5 \text{ mm} < D_p < 1.25 \text{ mm}$) was clearly observed. For the coarse particle the conversion achieved is around 80%. When using fine particles, the reaction reaches completion by the end of the reactor (99% conversion).

The second part of the research question is whether a microreactor can be used to help improve the kinetics of the reaction. Using the model it was shown that under the operating conditions mass transfer limitations play a significant role. Microreactors are being used to increase the gas-liquid interface area and should therefore be useful to increase the reaction rate. Also using a microreactor can allow for smaller catalyst particles to be used, which has been shown to improve the reaction rate. Unfortunately, given the limited time in the project, the reaction tests in microreactors have not been performed. However, a cold-flow test has shown that the slug flow pattern inner details in microreactors is dependent on the pressure, providing useful insights in designing packed-bed microreactors.

6 Recommendations for future research

For this study a method for accurate and reproducible sample analysis is needed. It appears that using NMR analysis doesn't give an accurate representation of the concentration in the sample. One way of solving this problem would be to use high pressure liquid chromatography, which could even be used on stream for real time analysis if resources are available.

Another recommendation would be to further analysis of the catalyst particle analysis using TEM microscopy to determine whether the crushing of the larger particles to obtain a fine powder affects the availability and stability of ruthenium on the active carbon.

To further investigate the gas transfer limitation the experiments can also be performed using a gas mixture instead of pure hydrogen. This will allow for change of the availability of hydrogen whilst keeping the gas-liquid ratio and the pressure constant.

7 Bibliography

- [1] J. J. Bozell and G. R. Petersen, "Technology development for the production of biobased products from biorefinery carbohydrates—the US Department of Energy's "Top 10" revisited," *Green Chem.*, vol. 12, no. 4, pp. 539-554, 2010.
- [2] J. van Haveren, E. L. Scott and J. Sanders, "Bulk chemicals from biomass," *Biofuels, Bioprod. Bioref.*, vol. 2, pp. 41-57, 2008.
- [3] K. Yan, C. Jarvis, J. Gu and Y. Yan, "Production and catalytic transformation of levulinic acid: A platform for speciality chemicals and fuels," *Renew Sustainable Energy Rev.*, vol. 51, pp. 986-997, 2015.
- [4] L. Deng, Y. Zhao, J. Li, B. Liao and Q. Guo, "Conversion of levulinic acid and formic acid into γ -valerolactone over heterogeneous catalysts," *ChemSusChem*, vol. 3, no. 10, pp. 1172-1175, 2010.
- [5] A. S. Piskun, d. J. E. Haan, E. Wilbers, v. d. H. H. Bovenkamp, Z. Tang and H. J. Heeres, "Hydrogenation of Levulinic Acid to γ -Valerolactone in Water Using Millimeter Sized Supported Ru Catalysts in a Packed Bed Reactor," *ACS Sustainable Chem. Eng.*, vol. 4, no. 6, pp. 2939-2950, 2016.
- [6] C. Ortiz-Cervantes and J. J. García, "Hydrogenation of levulinic acid to γ -valerolactone using ruthenium nanoparticles," *Inorg. Chim. Acta*, vol. 397, pp. 124-128, 2013.
- [7] C. Delhomme, L. A. Schaper, M. Zhang-Preße, G. Raudaschi-Sieber, D. Weuster-Botz and F. E. Kühn, "Catalytic hydrogenation of levulinic acid in aqueous phase," *J. Organomet. Chem.*, vol. 724, pp. 297-299, 2013.
- [8] K. Hengst, M. Schubert, H. W. P. Carvalho, C. Lu, W. Kleist and J. D. Grunwaldt, "Synthesis of γ -valerolactone by hydrogenation of levulinic acid over supported nickel catalysts," *Appl. Catal. A.*, vol. 502, pp. 18-26, 2015.
- [9] J. C. Serrano-Ruiz, D. Wang and J. A. Dumesic, "Catalytic upgrading of levulinic acid to 5-nonanone," *Green Chem.*, vol. 12, no. 4, pp. 574-577, 2010.
- [10] P. P. Upare, J. M. Lee, D. W. Hwang, S. B. Halligudi, Y. K. Hwang and J. S. Chang, "Selective hydrogenation of levulinic acid to γ -valerolactone over carbon supported noble metal catalysts," *J. Ind. Eng. Chem*, vol. 2011, no. 17, pp. 287-292, 2011.
- [11] J. Q. Bond, O. A. Abdelrahman and A. Heyden, "Analysis of Kinetics and reaction pathways in aqueous-phase hydrogenation of levulinic acid to form γ -valerolactone," *ACS Catalysis*, vol. 4, no. 4, pp. 1171-1181, 2014.
- [12] M. Sudhakar, V. V. Kumar, G. Naresh, M. L. Kantam, S. K. Bhargava and A. Venugopal, "Vapor phase hydrogenation of aqueous levulinic acid over hydroxyapatite supported metal (M= Pd, Pt, Ru, Cu, Ni) catalysts," *Appl. Catal. B.*, vol. 180, pp. 113-120, 2016.
- [13] A. S. Piskun, v. d. H. H. Bovenkamp, C. B. Rasrendra, J. G. M. Winkelman and H. J. Heeres, "Kinetic modeling of levulinic acid hydrogenation to γ -valerolactone in water using carbon supported Ru catalyst," *ACS Sustainable Chem. Eng.*, vol. 4, no. 6, pp. 2939-2950, 2016.
- [14] L. Deng, J. Li, D. Lai, Y. Fu and Q. guo, "Catalytic conversion of biomass-derived carbohydrates into gamma-valerolactone without using an external H₂ supply," *Angewandte Chem.*, vol. 48, no. 35, pp. 6529-6532, 2009.

- [15] H. Gao and J. Chen, "Hydrogenation of biomass-derived levulinic acid to γ -valerolactone catalyzed by PNP-Ir pincer complexes: A computational study," *J. Organomet. Chem.*, vol. 797, pp. 165-170, 2015.
- [16] V. V. Ranade, R. V. Chaudhari and P. R. Gunjal, *Trickle bed reactors reactor engineering applications*, Elsevier B.V., 2011.
- [17] J. Yue, G. Chen, Q. Yuan, L. Luo and Y. Gonthier, "Hydrodynamics and mass transfer characteristics in gas-liquid flow through a rectangular microchannel," *Chem. Eng. Technol.*, vol. 62, no. 7, p. 2096–2108, 2007.
- [18] J. Yoshida, A. Nagaki, T. Iwasaki and S. Suga, "Enhancement of chemical selectivity by microreactors," *Chem. Eng. Technol.*, vol. 28, no. 3, 2005.
- [19] S. Walter, S. Malmberg, B. Schmidt and M. A. Liauw, "Mass transfer limitations in microchannel reactors," *Cat. Tod.*, no. 110, pp. 15-25, 2005.
- [20] J. A. Moulijn, M. Makkee and R. J. Berger, "Catalyst testing in multiphase micro-packed-bed reactors; criterion for radial mass transport," *Cat. Today*, vol. 259, pp. 354-359, 2016.
- [21] A. Faridkhou and F. Larachi, "Hydrodynamics of Gas-Liquid cocurrent flows in micropacked Beds—Wall visualization study," *Ind. Eng. Chem*, vol. 51, no. 50, pp. 16495-16504, 2012.
- [22] A. Faridkhou and F. Larachi, "Two-phase flow hydrodynamic study in micro-packed beds – effect of bed geometry and particle size," *Chem. Eng. Process*, vol. 78, pp. 27-36, 2014.
- [23] S. Z. Rouhani and M. S. Sohal, "Two-phase flow patterns: A review of research results," *Prog. Nucl. Energ.*, vol. 11, no. 3, pp. 219-259, 1983.
- [24] J. M. Santos, T. R. Melli and L. E. Scriven, "Mechanics of gas-liquid flow in packed-bed contactors," *Annu. Rev. Fluid. Mech.*, vol. 23, no. 1, pp. 233-260, 1991.
- [25] Y. Taitel and D. Barnea, "Counter current gas-liquid vertical flow, model for flow pattern and pressure drop," *Int. J. Multiph. Flow*, vol. 9, no. 6, pp. 637-647, 1983.
- [26] P. Plouffe, D. M. Roberge and A. Macchi, "Liquid-liquid flow regimes and mass transfer in various micro-reactors," *Chem. Eng. J.*, vol. 300, pp. 9-19, 2016.
- [27] P. A. Ramachandran and R. V. Chaudhari, *Three-phase catalytic reactors*, Michigan: GordonBreach, 1983.
- [28] B. B. Hallac, K. Keyvanloo, Hecker, M. d. Argyle and M. D. Argyle, "An optimized simulation model for iron-based Fischer-Tropsch catalyst design: Transfer limitations as functions of operating and design conditions," *Chem. Eng. J.*, vol. 263, pp. 268-279, 2015.
- [29] H. S. Fogler, "Slurry reactors," in *Elements of Chemical Reaction Engineering*, Upper Saddle River, NJ, Prentice Hall, 2006, pp. 596-610.
- [30] H. S. Fogler, "Trickle bed reactor," in *Elements of Chemical Reaction Engineering*, Upper Saddle River, NJ, Prentice Hall, 2006, pp. 610-621.
- [31] S. Fukushima and K. Kusaka, "Liquid-phase volumetric mass transfer coefficient and boundary of hydrodynamics flow regime in packed column with co current downward flow.," *J. Chem. Eng. Jpn.*, vol. 10, no. 6, pp. 468-474, 1977.
- [32] J. C. Lagarias, *The Kepler Conjecture: The Hales-Ferguson Proof*, New York, USA: Springer New York, 2011.
- [33] I. Iliuta, F. Larachi, B. P. A. Grandjean and G. Wild, "Gas-liquid interfacial mass transfer in trickle-bed reactors: state-of-the-art correlations," *Chem. Eng. Sci.*, vol. 54, no. 23, pp. 5633-5645, 1999.

- [34] S. Fukushima and K. Kusaka, "Interfacial area and boundary of hydrodynamic flow region in packed column with cocurrent downward flow," *J. Chem. Eng. Jpn.*, vol. 10, no. 6, pp. 461-467, 1977.
- [35] R. J. Berger, J. Pérez-Ramirez, F. Kapteijn and J. A. Moulijn, "Catalyst performance testing: bed dilution revisited," *Chem. Eng. Sci.*, vol. 57, no. 22-23, pp. 4921-4932, 2002.
- [36] R. Sander, "Compilation of Henry's law constants (version 4.0) for water as solvent," *Atmos. Chem. Phys.*, vol. 15, pp. 4399-4981, 2015.
- [37] E. L. Cussler, *Diffusion Mass Transfer in Fluid Systems*, New York, USA: Cambridge University Press, 1997.
- [38] The international association for the properties of water and steam, "Release on the IAPWS Formulation 2008 for the Viscosity of Ordinary Water Substance," September 2008. [Online]. Available: <http://www.iapws.org/relguide/viscosity.html>. [Accessed 20 August 2016].
- [39] STREM, "<http://www.strem.com/catalog>," strem, 2016. [Online]. Available: http://www.strem.com/catalog/v/44-4000/59/ruthenium_7440-18-8. [Accessed 2016].
- [40] A. Faridkhou, M. Hamidipour and F. Larachi, "Hydrodynamics of gas-liquid micro-fixed beds – measurement approaches and technical challenges," *Chem. Eng. Journal*, vol. 223, pp. 425-435, 2013.
- [41] T. Daele, van, D. Fernandes del Poze, D. Hauwermeiren, van, K. V. Gerneay, R. Wohlgemuth and I. Nopens, "A generic model-based methodology for quantification of mass transfer limitations in microreactors," *Chem. Eng. J.*, no. 300, pp. 193-208, 2016.
- [42] K. D. Nagy, B. Shen, T. F. Jamison and K. F. Jensen, "Mixing and dispersion in smallscale flow systems," *Org. Process Res. Dev.*, vol. 16, no. 5, pp. 976-981, 2012.
- [43] P. P. Upare, J. M. Lee, D. W. Hwang, S. B. Halligudi, Y. K. Hwang and J. S. Chang, "Selective hydrogenation of levulinic acid to γ -valerolactone over carbon-supported noble metal catalysts," *J. Ind. Eng. Chem.*, vol. 17, pp. 287-292, 2011.

8 Appendix

8.1 Experimental overview:

Experiment A

Experiment	Goal	Conditions	Conversion (% of LA reacted)
A	Exploratory	Standard, with coarse particle	25
B	Exploratory	Standard, with coarse particle Fresh catalyst, new H ₂ flow regulator	64
C1	Exploratory	Standard, with coarse particle (re-used)	80
C2	Exploratory, halfway increase H ₂ flow	Standard, with coarse particle (re-used), after 90 min increase hydrogen flow to 50 mL/min	78
C3	Exploratory, lower liquid flow	Standard, liquid flow: 0.6 ml/min	83
D3	High pressure, high gas flow (increased hydrogen concentration)	Gas flow: 40 ml/min; pressure: 60 bar; liquid flow: 10 ml/min	90
E	No hydrogen (testing water evaporation in standard run)	Standard, but no gas flow	0
F1	Fine catalyst	Standard, fine catalyst	99
F2	Fine catalyst, lower temperature	Standard, Temperature: 80 °C	93
F2'	Fine catalyst, lower temperature	Standard, Temperature: 70 °C	96
G	Low residence time (higher liquid and gas flows)	Standard, pressure: 60 bar; gas flow: 45 ml/min; liquid flow: 1.2 ml/min	98

Table 14, conversion for initial experiments (standard conditions where used for all experiments unless stated differently).

Experiment	Conditions (weight in grams)	Conversion (%)
Ha	Catalyst weight: 1.64; Filler weight: 0.21	98.29
Hb	Catalyst weight: 1.39 Filler weight:0.49	98.62
Hc	Catalyst weight: 1.21 Filler weight: 0.74	51.72
Hc2	Catalyst weight: 1.22 Filler weight:0.58	96.65
Hd	Catalyst weight: 0.89 Filler weight: 1.01	65.63
He	Catalyst weight: 0.58 Filler weight: 1.30	44.40
He2	Catalyst weight: 0.61 Filler weight:1.20	85.57
Hf	Catalyst weight: 0.41 Filler weight:1.38	54.07
Hf2	Catalyst weight: 0.41 Filler weight:1.41	61.61
Hg	Catalyst weight: 0.78 Filler weight:1.03	85.54

Table 15, conversion for experiment set H (standard conditions where used for all experiments unless stated differently).

8.2 Values for used parameters

Parameter	Correlation	Value	Unit	Source
Henry constant	H	0.014	kg _{gas} /kg _{water}	[36]
Reactor volume	V	4E-6	m ³	measured
Diffusivity	D in water (at p=1 bar and T= 25 °C)	4.5E-5	m/s	[37]
Superficial liquid velocity	U _L = liquid volume flow per area	1.67	m/s	measured
dynamic viscosity liquid	μ _L	3.5E-4	kg/(m*s)	[38]
Liquid density	ρ _L	10E3	kg/m ³	assumed
area /mass	$a_c = \frac{6}{d_p \rho_p}$	5.00E-3	g/m ²	[30]
particle diameter	d _p	6E-4	m	measured
Particle density	supplier specified		kg/m ³	[39]
Effectiveness factor	η	range 0 - 1		

Table 16, typical values and correlations for parameters in Equation 8 and Equation 10.

8.3 Flow pattern dependency on pressure

Below the photographs are shown used for the flow pattern dependency in the microreactor as discussed in paragraph 4.3.2. The gas flow is 20 ml/min at standard conditions and the liquid flow: 0.6 ml/min. The pressure is shown in the caption below.



Figure 24, pressure: 8 bar, photo 1.



Figure 25, pressure: 8 bar, photo 2.



Figure 26, , pressure: 12 bar, photo 1.



Figure 27, , pressure: 12 bar, photo 2.



Figure 28, pressure: 20 bar, photo 1.



Figure 29, pressure: 20 bar, photo 2.



Figure 30, pressure: 20 bar, photo 3.



Figure 31, pressure: 25 bar, photo 1.



Figure 32, pressure: 25 bar, photo 2.



Figure 33, pressure: 35 bar, photo 1.



Figure 34, pressure: 35 bar, photo 2.



Figure 35, pressure: 40 bar, photo 1.



Figure 36, pressure: 40 bar, photo 2.



Figure 37, pressure: 40 bar, photo 3.



Figure 38, pressure: 45 bar, photo 1.



Figure 39, pressure: 45 bar, photo 2.

8.4 Particle analysis

The pictures used for the characterization of the powder mixtures are shown below. Figure 40 and Figure 41 show used catalyst and filler mixtures. Figure 42 and Figure 43 show fresh fine catalyst. Figure 44 and Figure 45 are depictions of fresh coarse catalyst. Figure 46 and Figure 47 show the filler material (SiC).

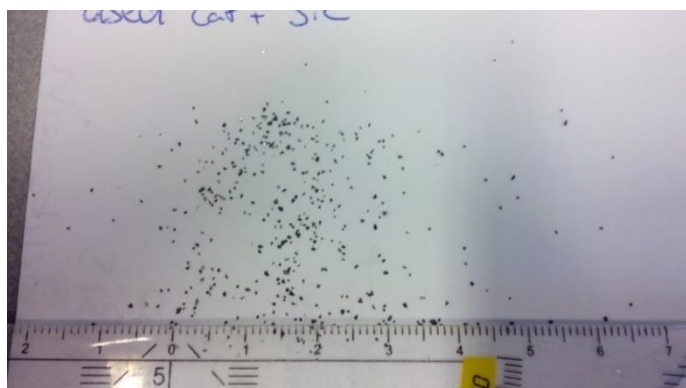


Figure 40, used fine catalyst and filler (1).



Figure 41, used fine catalyst and filler (2).



Figure 42, fresh fine catalyst (1).



Figure 43, fresh fine catalyst (2).



Figure 44, fresh coarse catalyst (1).



Figure 45, fresh coarse catalyst (2).

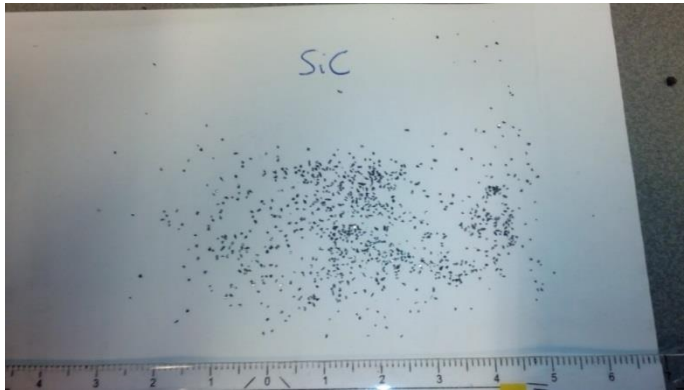


Figure 46, fresh filler (SiC) (1).

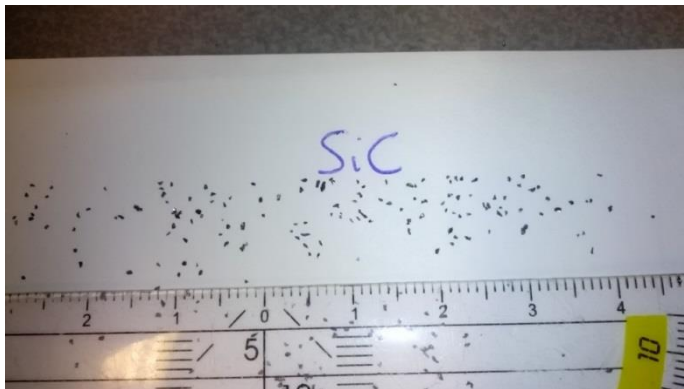


Figure 47, fresh filler (SiC) (2).